Master thesis

Formation of heat resistant Ni silicide by additional Hf layers

Supervisor

Professor Hiroshi Iwai

Tokyo Institute of Technology

Department of Advanced Applied Electronics

03M36145

Youichi Kobayashi

Contents

Chapter 1

Introduction

In this chapter, we described research background, transition of electrode materials, selecting additives for Ni silicide and the purpose of this study.

1.1 Research background

The continuous development of techniques for the formation of thin films and more advanced microfabrication processes have resulted in higher performance and integration density for Si ULSI systems. In recent years, the minimum line width for actual device generations has reached less than 100nm. Considering the different materials found between the metal electrodes and semiconductor devices, the ultra shallow junctions formed at source and drain areas are then accompanied with non heterogeneities at these junction interfaces. As the contact area becomes smaller, the contact resistivity increases and this problem tend to be worsened for even shallower junctions. Figure 1-1 shows (a) contact silicide thickness and (b) contact resistivity demanded in the future.

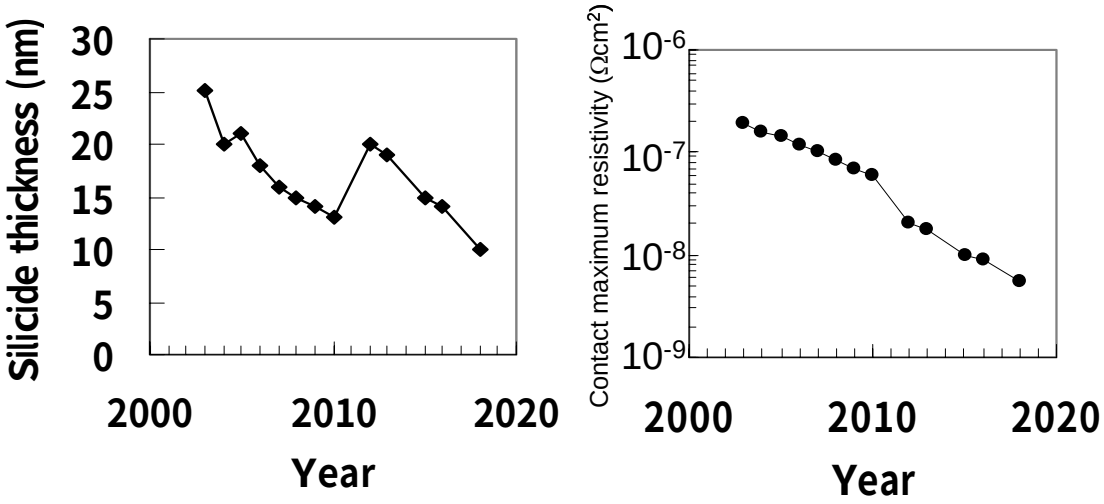

(a) (b)

Fig.1-1 Roadmap of (a) contact silicide thickness and (b) contact resistivity [1]

Therefore, it is indispensable element to establish formation technology of ultra low resistance and ultra flat metal silicide / Si interface, in order to realize new generation of global integration devices, which are integrated with high density in ultra high speed and low power consumption devices of next generation. In particular, it is demanded to achieve ultra flat contact which has low contact resistivity of about $10^{-8}\Omega cm^2$, high thermal stability.

1.2 Transition of electrode materials

Historically gate electrode materials of MOS transistor in semiconductor industry started using aluminum of pure metal. Thus, parasitic resistance did not become a problem. However, aluminum was not able to obtain heat resistance to form source and drain. For this reason, polysilicon gate technology which had heat resistance was developed. But polysilicon was difficult to reduce layer resistance if it was doped with high concentration impurities. Hence, from the view point of high temperature heat treatment, WSi_2 and $MoSi_2$ silicide were used for gate electrode materials.

Dual gate CMOS process to achieve threshold control of CMOS transistor was demanded when transistor size became 0.25~0.35μm. However, mutual diffusion of impurities in gate electrode interface became serious problems for WSi_2 polycide gate. Therefore, salicide technology which suppressed mutual diffusion of impurities in gate electrode was required. Figure 1-2 shows process of formation for Ni salicide.

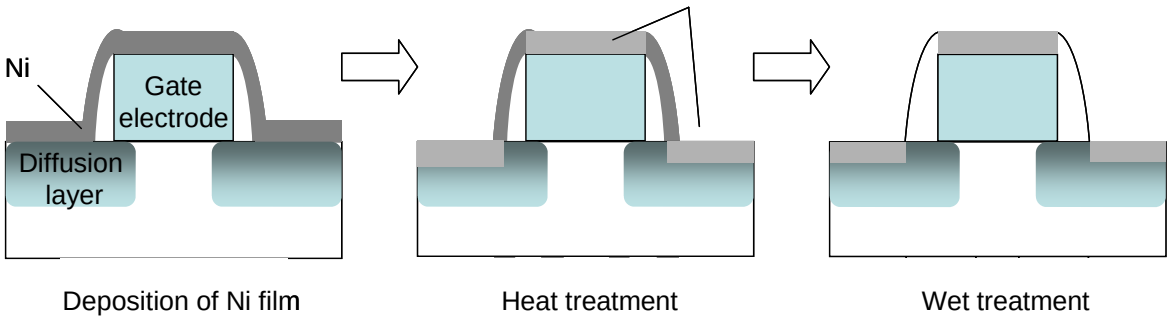

Fig.1-2 Process of formation for Ni salicide

In salicide technology, Ti silicide ($TiSi_2$) was initially adopted as low-resistance silicide. However, for $TiSi_2$, the transformation from the metastable high resistivity C49-$TiSi_2$ phase to the thermodynamically stable low resistivity C54-$TiSi_2$ phase is nucleation limited [2~4], causing linewidth dependence of the sheet resistance for lines narrower than 0.35μm.

In order to resolve this problem, Co silicide ($CoSi_2$) was selected on account of the following when transistor size became 65~180nm.

1) Phase transition does not occur as $TiSi_2$.

2) Melting point is high.

3) linewidth effects are not observed more than 50nm.

Various researches have been continued in order to actualize transistor size under 65nm recently. Junction leakage, a relatively large consumption of Si, and the difficulty in producing a uniform silicide layer seem to be limiting factors for the application of a Co salicide process to deep submicrometer devices [5]. For

ULSI applications, NiSi is a most promising silicide material due to its low resistivity, less Si consumption, low silicidation temperature, and relative linewidth-independent sheet resistance of the gate electrode [6~8].

1.3 Selection of additives for Ni silicide

In subchapter 1.2, we described effectiveness of NiSi. However, NiSi is not the final stable phase for the Ni/Si reaction system. NiSi agglomeration takes place and its phase transformation from NiSi to $NiSi_2$ occurs during high heat treatment [9~10]. Thus, various additives which improve thermal stability are investigated in order to resolve these problems.

Recently, great efforts have been made to study the thermal stability of NiSi, reportedly being improved by use of a thin Pt [11~15], Pd [16~18], and Co [19] interlayer between the Ni film and Si substrate. It is expected to prevent that Ni diffused to Si substrate through the interface layer because these materials have strong reactivity with Si. In other words, barrier layer reacts with Si to form silicide in first. As a result, barrier layer prevent NiSi from changing to $NiSi_2$.

Figure 1-3 shows conceptual diagram of materials which have strong reactivity with Si.

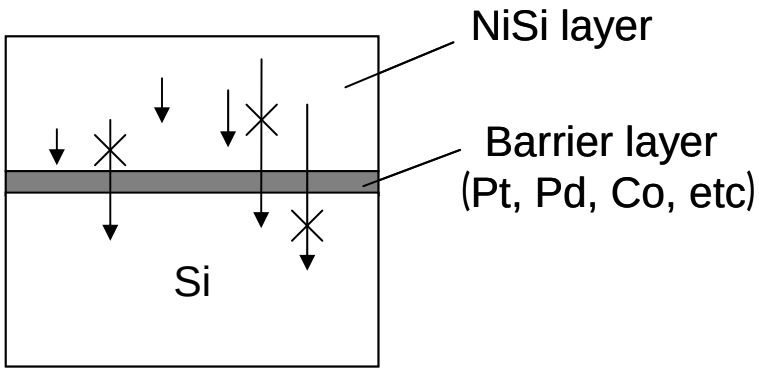

Fig.1-3 Conceptual diagram of materials which have strong reactivity with Si.

On the other hand, recently, much study has also shown that, during silicidation, NiSi is extremely sensitive to oxygen contamination which could be suppressed by adding a Zr capping layer [20]. The increase of interface energy generally enhances agglomeration of NiSi at lower temperature when no capping layer exists. Thus, It is considered that the surface energy decreases largely enough to compensate the increase of interface energy by Zr capping layer, which has weak reactivity with Si. Figure 1-4 shows conceptual diagram of materials which have weak reactivity with Si.

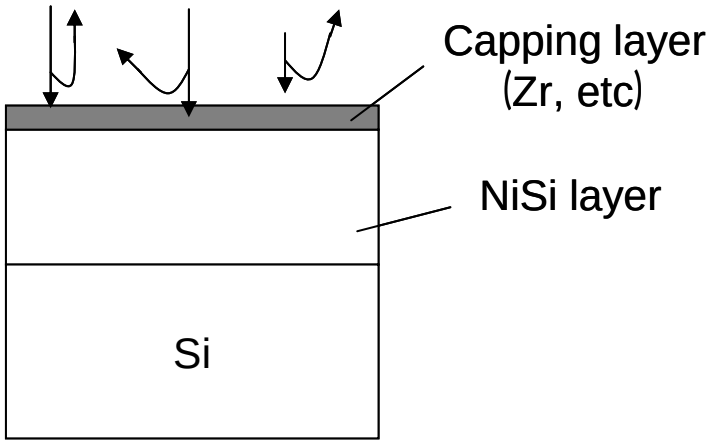

Fig.1-4 Conceptual diagram of materials which have weak reactivity with Si.

1.4 Purpose of this study

NiSi is the main candidate for replacing $TiSi_2$ and $CoSi_2$ as the contact material in advanced integrated circuits. However, NiSi has an issue with thermal stability, that is, NiSi has high resistivity at high temperatures due to phase transformation from NiSi to $NiSi_2$ or agglomeration of the silicide layers. Recently, great efforts have been made to study the thermal stability of NiSi, reportedly being improved by use of Pt, Pd, Ir and Co additives. Thus, the purpose of this study is to improve thermal stability of NiSi by additional Hf layers.

Chapter 2

Fabrication and Characterization Method

2.1 Fabrication methods

In this sub section, the fabrication methods for Ni silicide were discussed.

2.1.1 Chemical cleaning of Si substrate

Prior to silicide metal deposition, Si substrate was chemically cleaned to remove impurities and particles from the surface.

Ultra-pure water (UPW) systems used in this study, the provided UPW with more than 18.2 MO・cm resistively. UPW is highly purified and filtered to remove all traces of ionic, particulate, and bacterial contamination.

In this study, the substrate cleaning process was so designed as to control the ultra-clean Si surface, which was given in Figure 2-1. First, the conventional chemical cleaning using SPM solution (sulfuric acid (H_2SO_4): hydrogen peroxide (H_2O_2) = 4:1) was performed to remove any organic material and metallic impurities. And then, the substrates dipped in hydrofluoric acid (HF) for 5 min to remove the native or chemical oxide. Finally, the cleaned wafer was dipped in UPW and loaded to chamber immediately (HF-last).

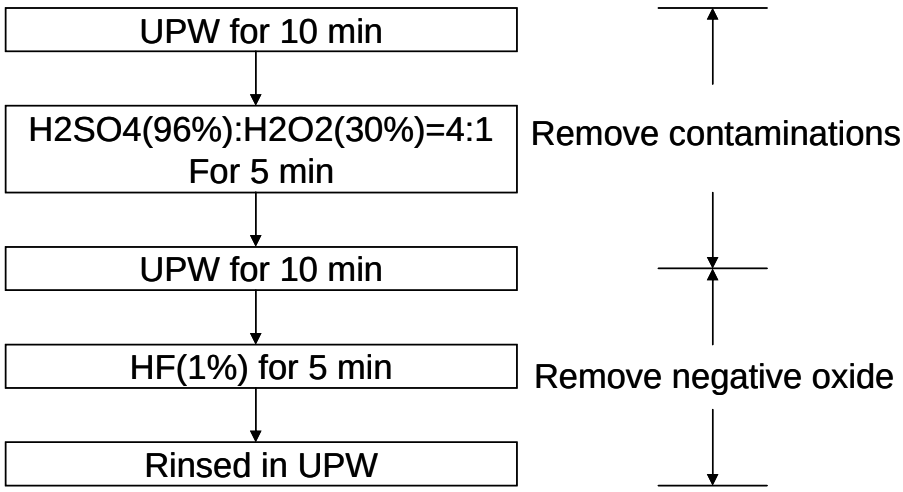

Fig.2-1 Cleaning process of Si substrate

2.1.2 The Sputtering System

In this study, sputtering method using sputtering equipment was employed for silicide metal deposition. Figure 2-17 shows the sputtering system. Within the sputtering process gas ions out of plasma are accelerated towards a target consisting of the material to be deposited. Material is detached from the target and afterwards deposited on a substrate in the vicinity. At this time, the magnetic field with the magnet by the side of the negative pole carries out the duty which gathers sputtering efficiency. The process is realized in a closed recipient, which is pumped down to a vacuum base pressure before deposition starts.

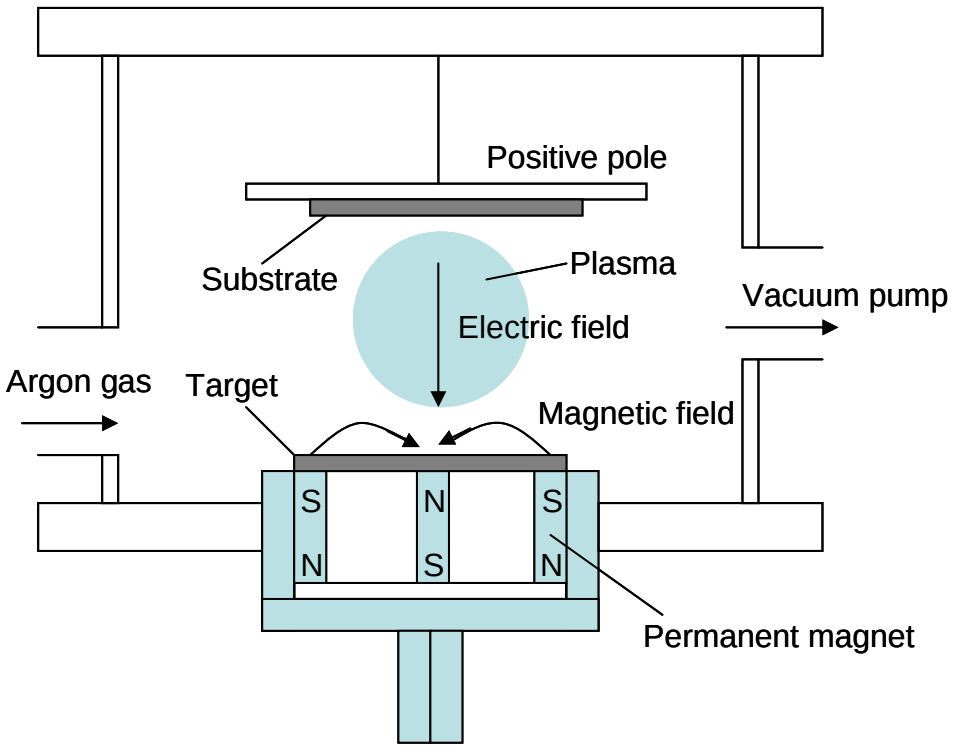

Fig.2-2 Schematic drawings of sputtering equipment

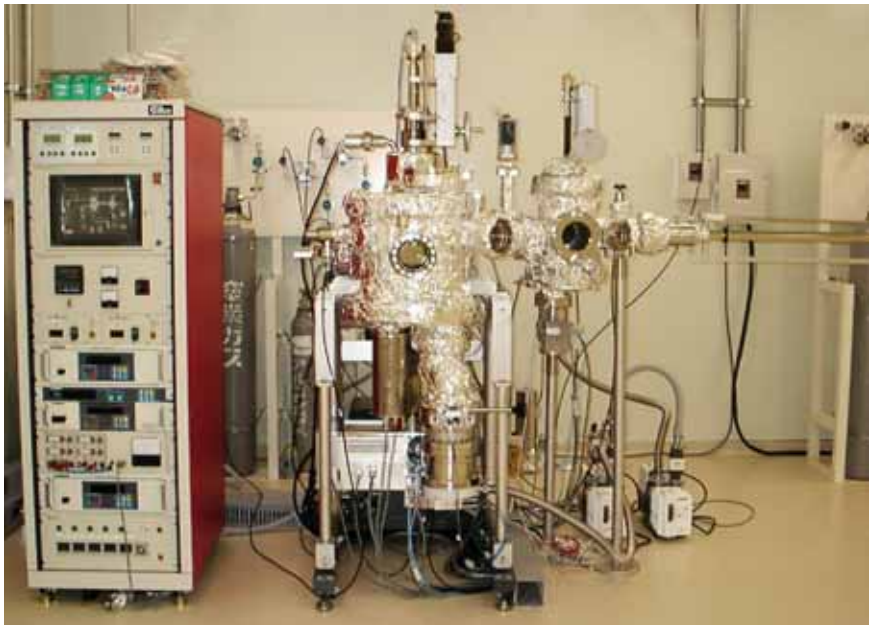

Fig.2-3 photograph of sputtering system

2.1.3 Rapid Thermal Anneal (RTA)

RTA (Rapid Thermal Anneal) equipment (QHC-P610, ULVAC Co. Ltd.) was used for annealing sample of after metal deposition. The schematic diagram is shown in Figure 2-4. The temperature was controlled by PID controller. Before the annealing, the ambient of the furnace was replaced with N_2 and H_2N_2 gas.

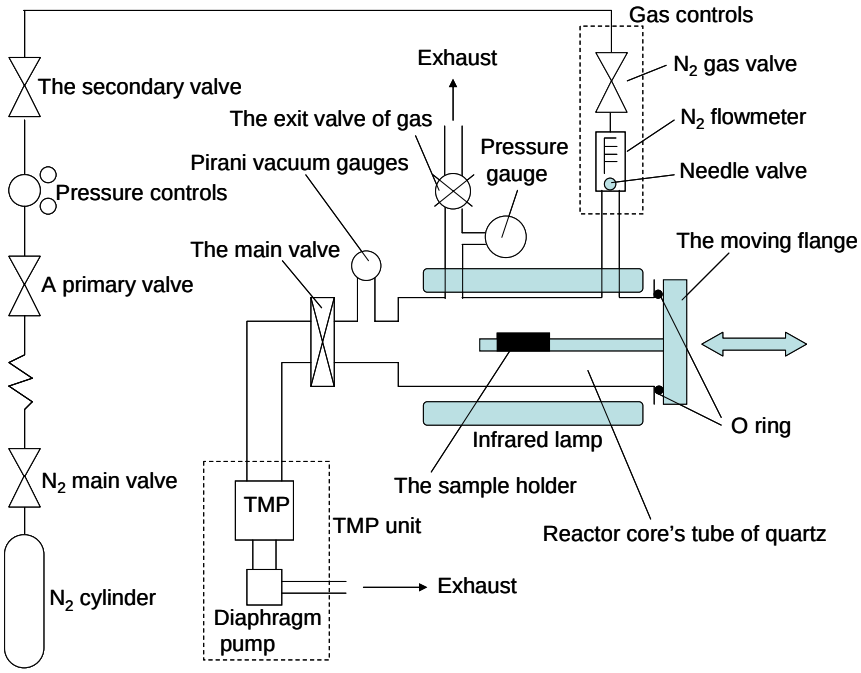

Fig.2-4 Schematic drawings of RTA equipment

Fig.2-5 Photograph of RTA equipment

2.2 Characterization methods

In this sub section, the characterization methods for Ni silicide are discussed.

2.2.1 Four-Point Probe Method

The resistivity of metal silicide was evaluated by four-point probe method. The schematic diagram was shown in figure 2-6. A small current (I) is passed though two outer probes and Voltage (V) is measured between the two inner probes. For an arbitrarily shaped sample the sheet resistance (ρ_{sh}) is given by

$$\rho_{sh} = \frac{V}{I} \times CF$$

where CF is correction factor that depends on the sample geometry. If distance between probes (s; in this study, s=1 mm) is very shorter than width of a sample (d), CF equals to π/ln(2)=4.54.

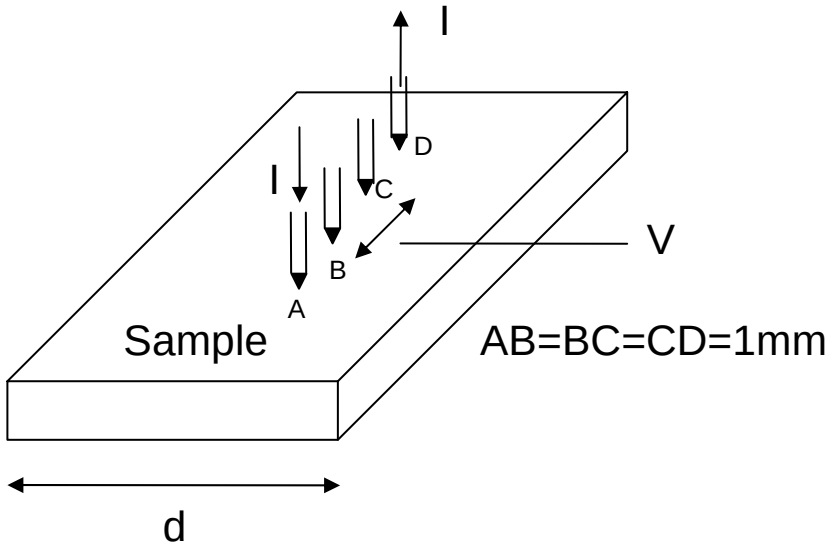

Fig.2-6 Schematic drawings of four-point probe method

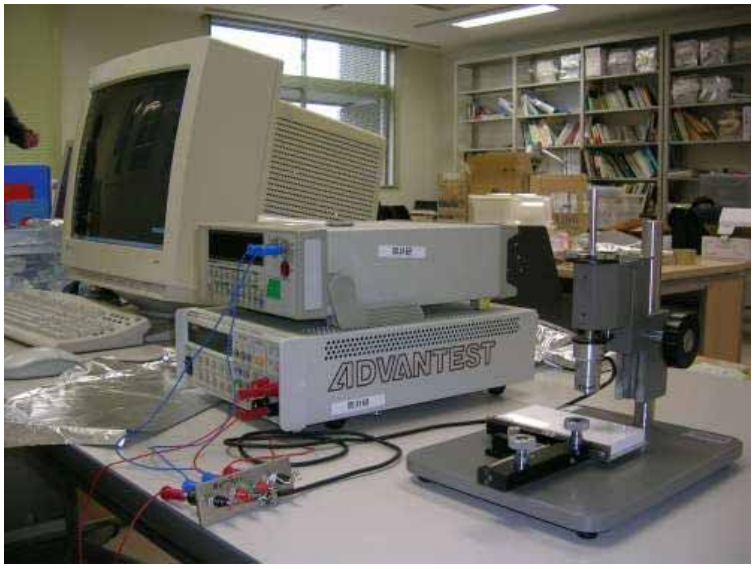

Fig.2-7 Photograph of four-point probe system

2.2.2 Rutherford Backscattering Spectrometry (RBS) method

Monoenergetic light ions, for example 2-MeV He ions, impinge on a sample. A very small portion of the ions will undergo head-on collisions with the nucleon of a sample atom on the surface as well as in-depth and backscattered. The scattering process (Rutherford scattering) can be represented as a simple two-body collision. This scattering event is so rare that the attenuation of the beam intensity on its path into the target is insignificant and the effect is usually ignored. The backscattered particles will escape the sample can be energy-analyzed. The backscattering energy distribution of the particles carries information on the mass and depth distribution of the target atoms where

scattering occurs, hence the depth profile of the sample. A scheme is shown in figure 2-8.

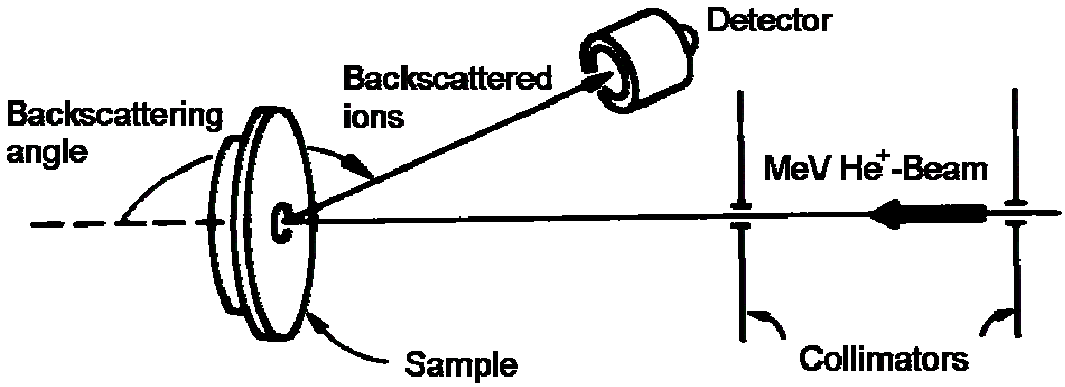

Fig.2-8 Schematic drawings of RBS method

Fig.2-9 Photograph of RBS equipment

2.2.3 Scanning Electron Microscope (SEM)

Figure 2-10 shows Scanning electron Microscope (SEM) system. The Virtual Source at the top represents the electron gun, producing a stream of monochromatic electrons. The stream is condensed by the first condenser lens. This lens is used to both form the beam and limit the amount of current in the beam. It works in conjunction with the condenser aperture to eliminate the high-angle electrons from the beam. The beam is then constricted by the condenser aperture, eliminating some high-angle electrons. The second condenser lens forms the electrons into a thin, tight, coherent beam. A user selectable objective aperture further eliminates high-angle electrons from the beam. A set of coils then scan or sweep the beam in a grid fashion, dwelling on points for a period of time determined by the scan speed. The final lens, the Objective, focuses the scanning beam onto the part of the specimen desired. When the beam strikes the sample, interactions occur inside the sample and are detected with various instruments interactions. Before the beam moves to its next dwell point these instruments count the number of interactions and display a pixel on a CRT whose intensity is determined by this number. This process is repeated until the grid scan is finished and then repeated, the entire pattern can be scanned 30 times per second.

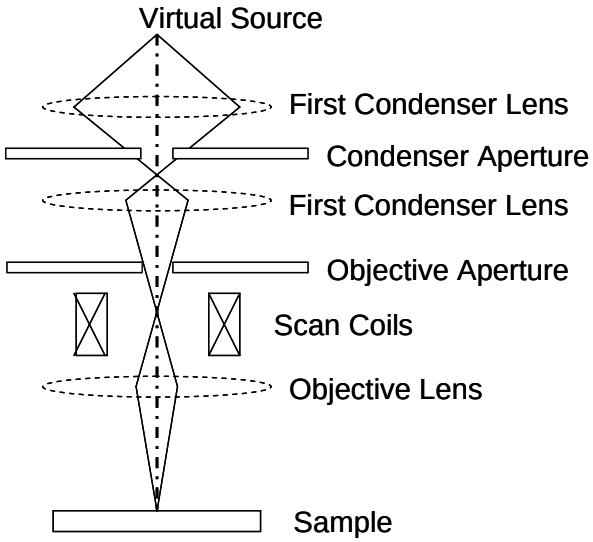

Fig.2-10 Schematic drawings of SEM equipment

Fig.2-11 Photograph of SEM equipment

2.2.4 Atomic Force Microscopy (AFM)

AFM enables to measure surface morphology by using force between atoms and approached tip. Surface roughness of a sample is observed correctly by the scanning in x and y directions. Figure 2-12 shows the principle of AFM.

Tip is vibrated during measurement, and displacement of z direction is detected. This method is called tapping mode AFM (TM-AFM). Resolution limit for normal AFM is 5~10nm depending on distance between sample surface and tip. On the other hand, resolution limit for TM-AFM is depended on size of tip edge. Thus, resolution limit for TM-AFM is about 1nm.

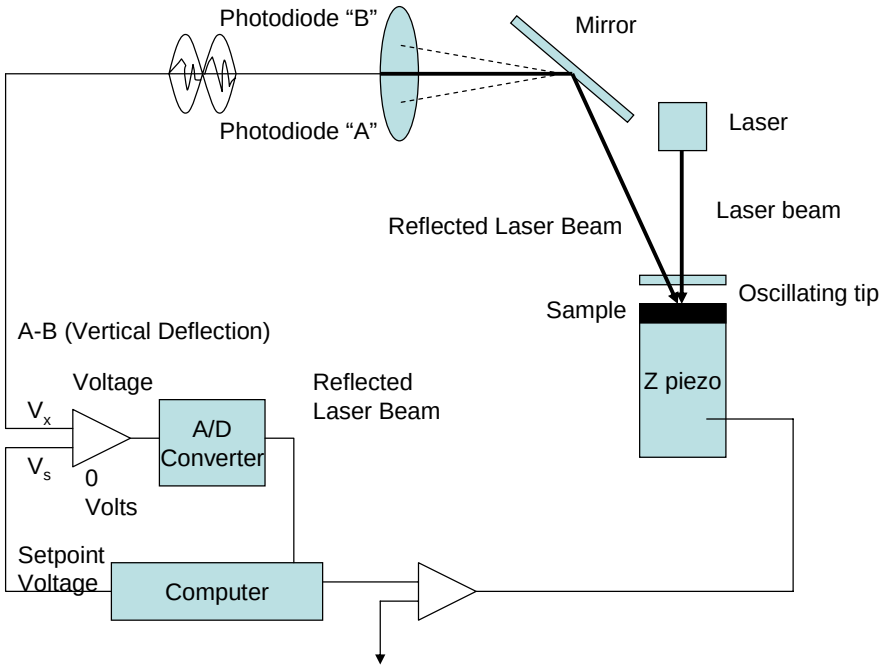

Fig.2-12 Schematic drawings of SEM equipment

Fig.2-13 Photograph of AFM equipment

Chapter 3

The sputtering rate measurement, temperature proofreading of annealing furnace and dependence of annealing rate

3.1 Introduction

In this chapter, we investigated metal deposition rate of sputtering system, which was used during metal deposition and temperature proofreading of annealing furnace after metal deposition. Finally, we also researched into dependence of annealing rate.

3.2 The sputtering rate measurement

In this study, we have to grasp metal deposition rate of sputtering system, in order to evaluate thin film in the order of nm. The parameter related to a deposition rate has DC power supply, distance from target to sample and deposition time. In this experiment, two parameters were fixed and metal deposition rate was measured with changing one of the remaining parameter.

3.2.1 The experiment method

The experiment methods are as follows.

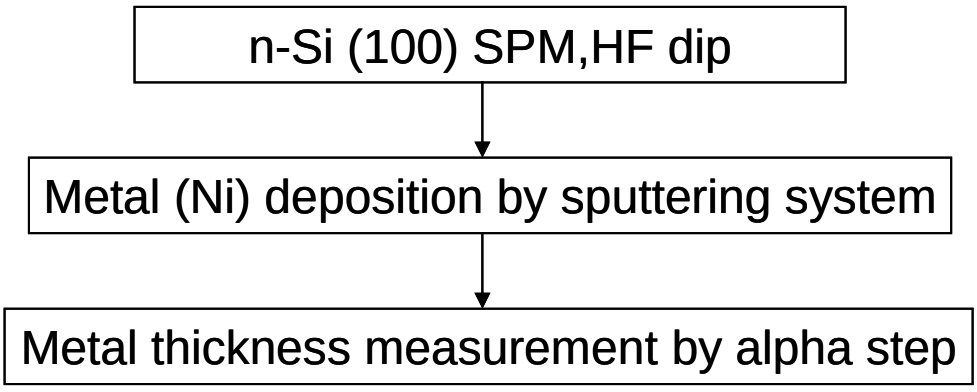

Fig.3-1 Experiment method of the sputtering rate measurement

3.2.2 Experiment result

Figure 3-2 shows film thickness as a function of power. At this time, distance is 100mm and time is 6 minute. It was observed that film thickness became thicker as power became larger.

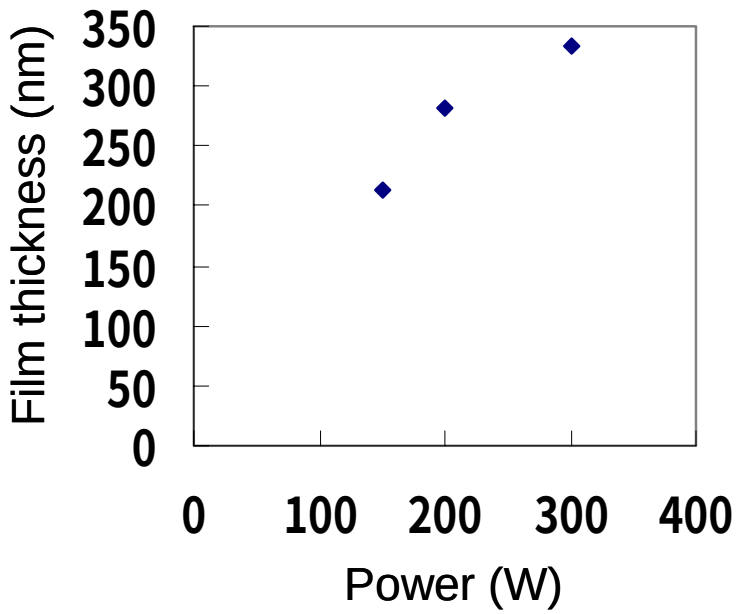

Fig.3-2 Depending on film thickness against power

Figure 3-3 shows film thickness as a function of distance. At this time, time is 6 minute and power is 300W. It was observed that film thickness became thinner as distance became longer.

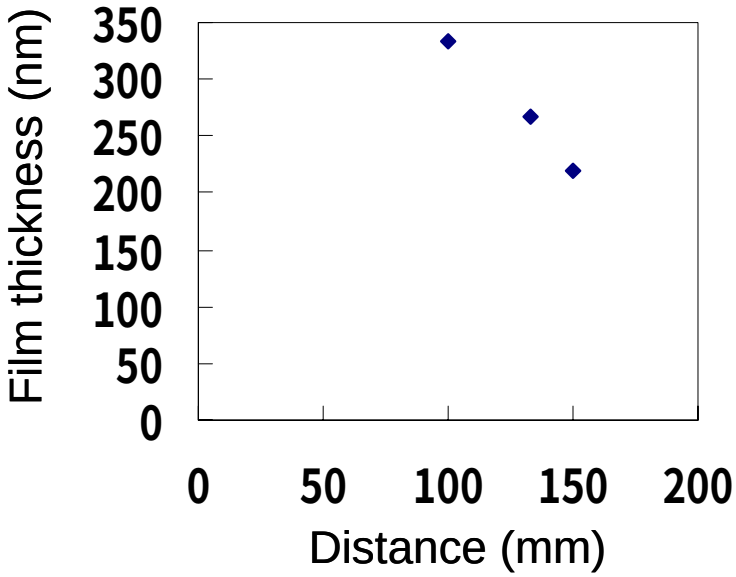

Fig.3-3 Depending on film thickness against distance

Figure 3-4 shows film thickness as a function of time. At this time, power is 300W and distance is 100mm. It was observed that film thickness became thicker as time became longer.

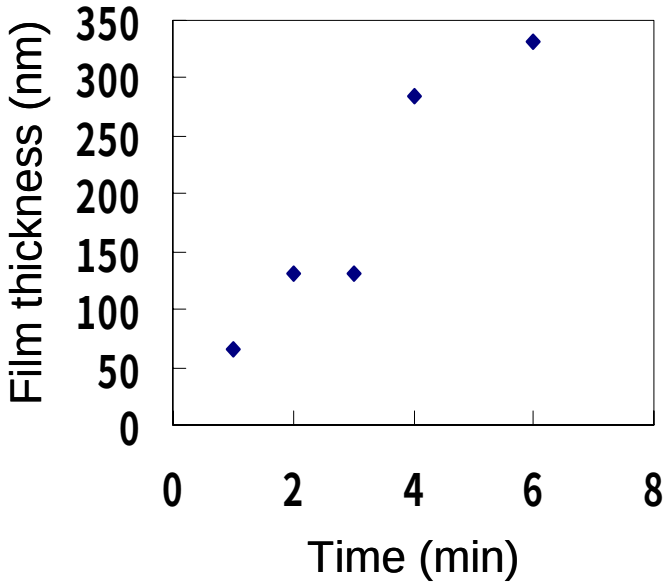

Fig.3-4 Depending on film thickness against time

3.3 Temperature proofreading of annealing furnace

Figure 3-5 shows the annealing furnace structure. In figure 3-5, thermocouple is put into carbon susceptor. Therefore, thermocouple temperature is equal to carbon susceptor temperature. But sample temperature is not equal to carbon susceptor temperature because of RTA. In fact, sample temperature is not equal to thermocouple temperature.

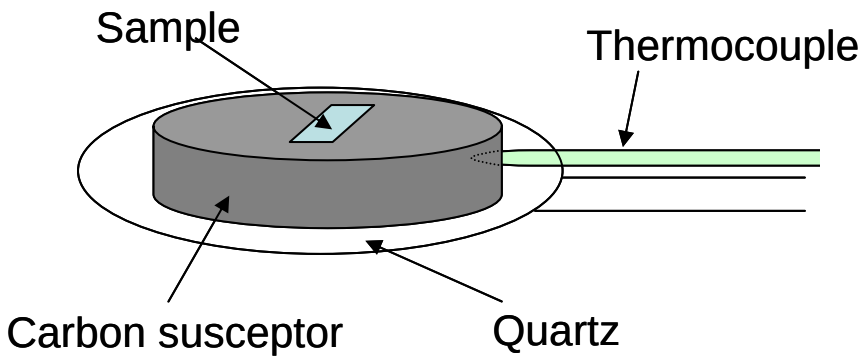

Fig.3-5 Structure of annealing furnace

In order to solve this problem, we consider new structure of annealing furnace in figure 3-6. In this structure, the whole sample is heated equally. However, it is possible that temperature display of thermocouple compares differently with sample temperature, because of thermocouple is not covered. Hence it is necessary to conduct temperature proofreading.

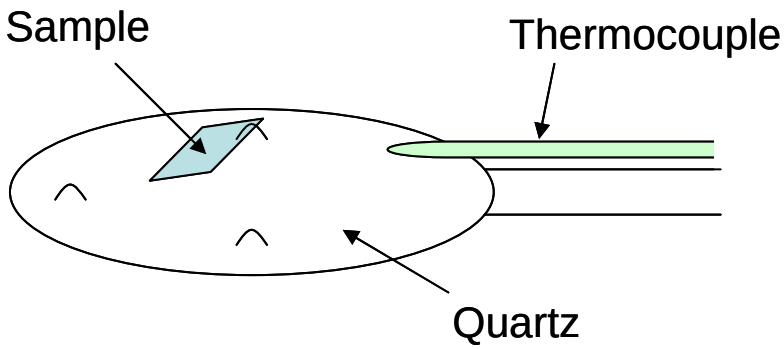

Fig.3-6 New structure of annealing furnace

3.3.1 The experiment method

The experiment methods are as follows.

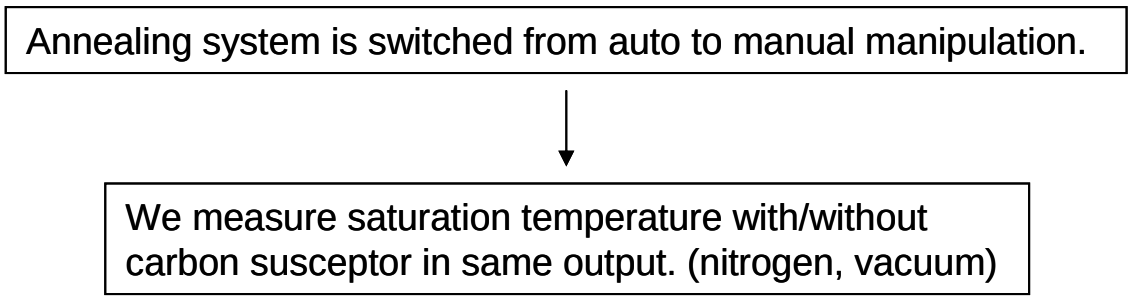

Fig.3-7 Experiment method of temperature proofreading of annealing furnace

3.3.2 Experiment result

Figure 3-8 shows display temperature of thermocouple as a function of output percent. In case of figure 3-8 (a), display temperature of thermocouple was almost equivalent in nitrogen and a vacuum. However, in case of figure 3-8 (b), display temperature of thermocouple in nitrogen was lower than in a vacuum if it was the same output percent.

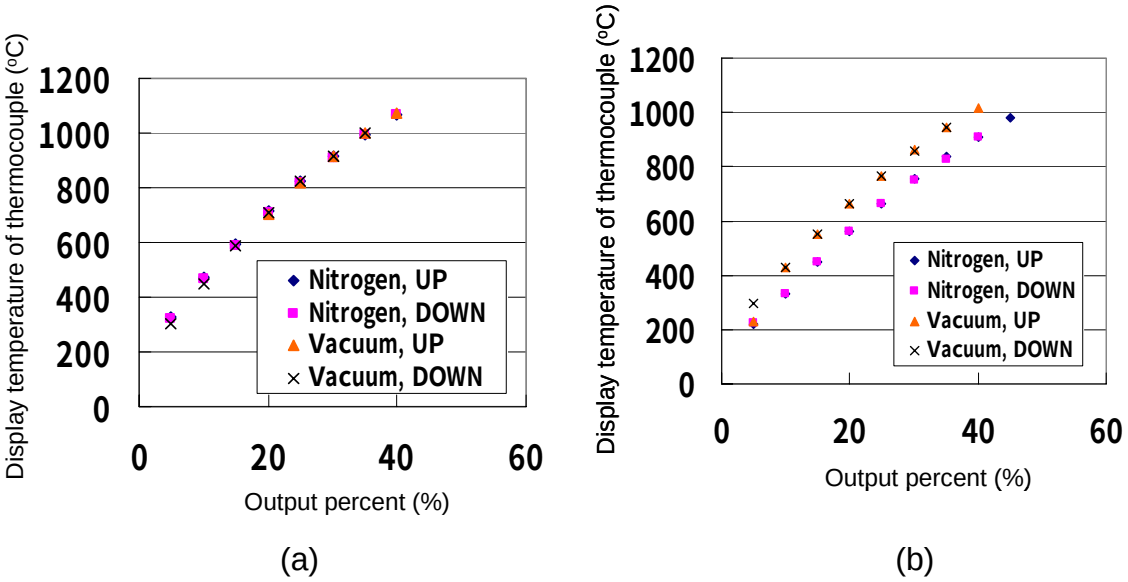

Fig 3-8 Display temperature of thermocouple vs. output percent of annealing furnace for (a) with susceptor and (b) without susceptor.

Figure 3-9 shows display temperature of thermocouple with susceptor as a function of display temperature of thermocouple without susceptor. Figure 3-9 was derived from figure 3-8. Hereafter, figure 3-9 is used to proofread temperature in RTA.

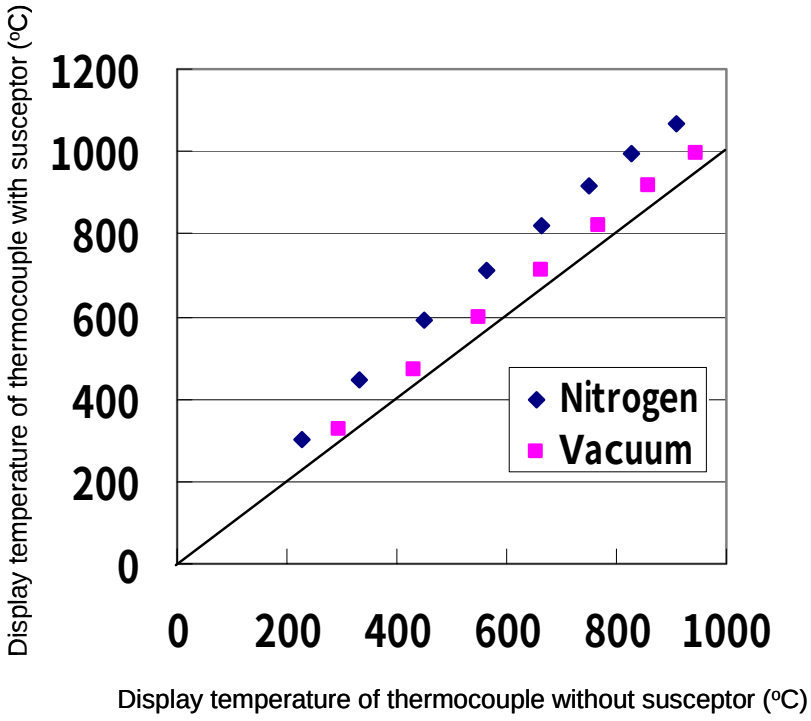

Fig 3-9 Display temperature of thermocouple with susceptor vs. without susceptor in same output.

3.4 Dependence on annealing rate

In this subchapter, we investigated dependence on annealing rate. As the reason for inquiring into dependence on annealing rate, there is overshoot. Figure 3-10 is a view showing a frame format of rapid thermal annealing (RTA) conditions.

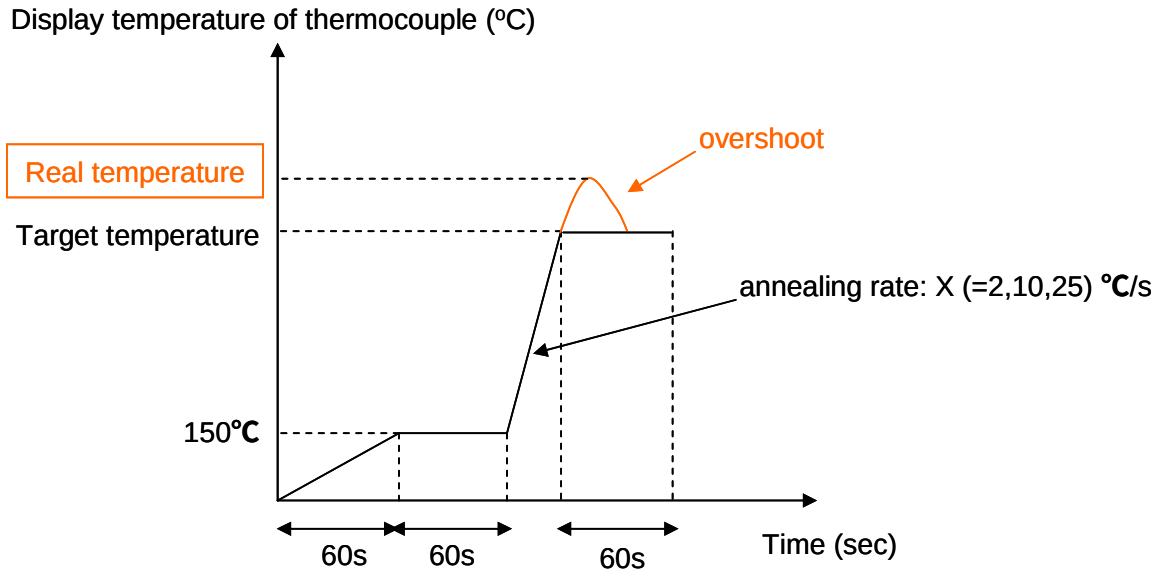

Fig.3-10 Pattern diagrams of RTA conditions

3.4.1 The experiment method

The experiment methods are as follows.

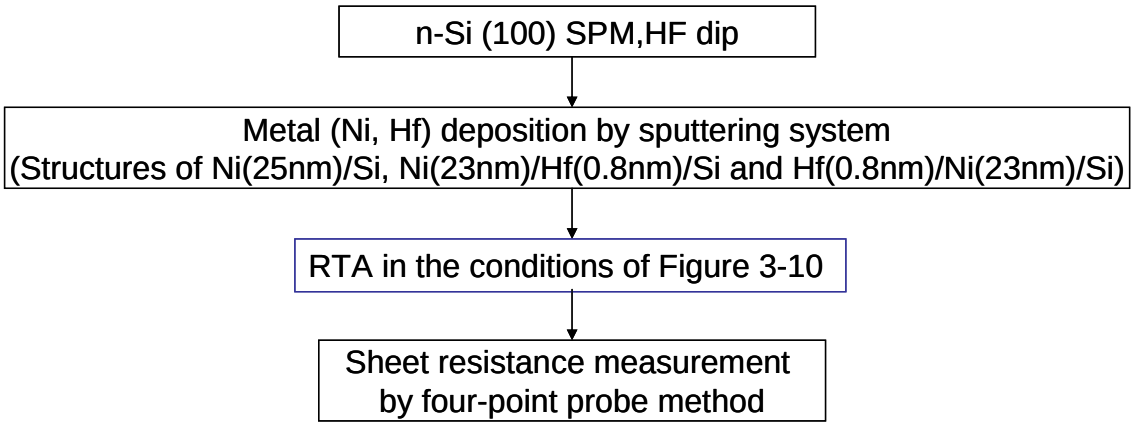

Fig.3-11 Experiment method of dependence on annealing rate

3.4.2 Experiment result

Figure 3-12 shows sheet resistance as a function of display temperature of thermocouple at a rate of 25^{o}C/s in forming gas (3%-H_2) ambient. It was found that critical temperature at which sheet resistance was 425^{o}C for the deposited structure of Ni(25nm)/Si and Ni(23nm)/Hf(0.8nm)/Si. Also it was found that critical temperature at which sheet resistance was 450^{o}C for the deposited structure of Hf(0.8nm)/Ni(23nm)/Si.

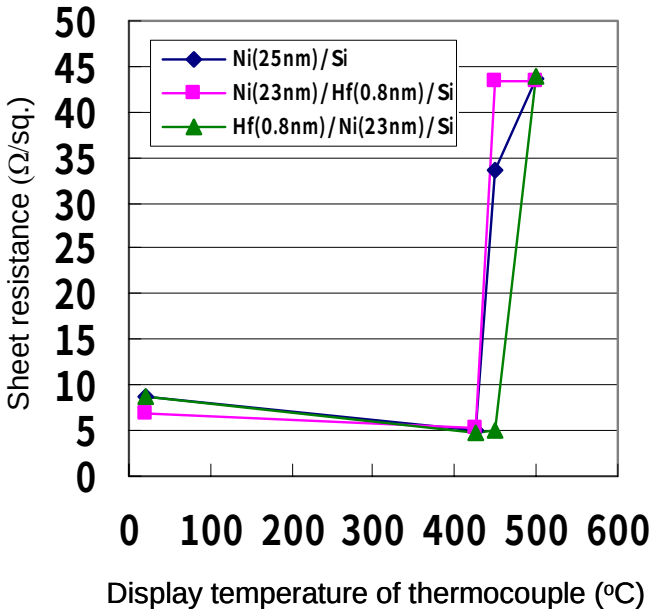

Fig.3-12 Sheet resistance vs. display temperature of thermocouple for Ni/Si, Ni/Hf/Si and Hf/Ni/Si structures at a rate of 25^{o}C.

Figure 3-13 shows sheet resistance as a function of display temperature of thermocouple at a rate of 10^{o}C/s in forming gas (3%-H_2) ambient. It was found that critical temperature at which sheet resistance was 450^{o}C for the deposited structure of Ni(25nm)/Si. While Hf(0.8nm)/Ni(23nm)/Si structure retained low resistance at 500^{o}C.

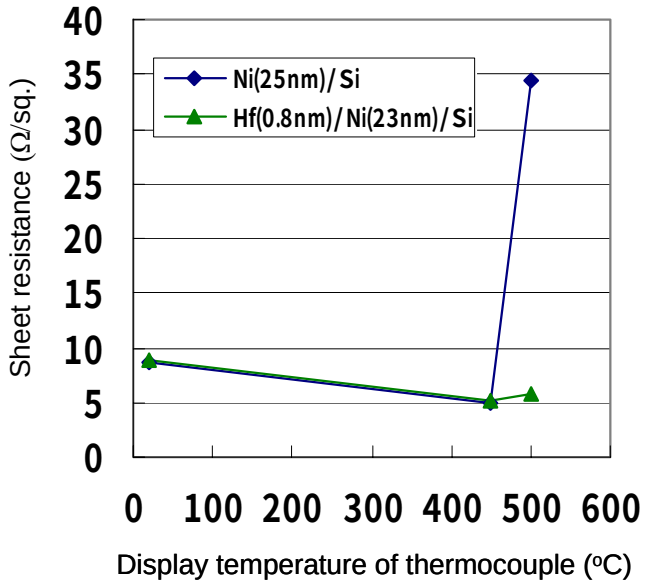

Fig.3-13 Sheet resistance vs. display temperature of thermocouple for Ni/Si and Hf/Ni/Si structures at a rate of 10^{o}C.

Figure 3-14 shows sheet resistance as a function of display temperature of thermocouple at a rate of 2^{o}C/s in forming gas (3%-H_2) ambient. It was found that critical temperature at which sheet resistance was 600^{o}C for the deposited structure of Ni(25nm)/Si and Hf(0.8nm)/Ni(23nm)/Si.

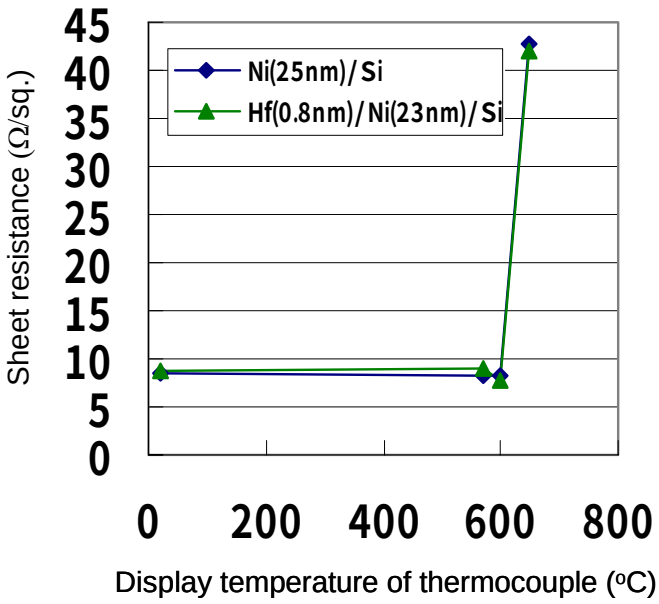

Fig.3-14 Sheet resistance vs. display temperature of thermocouple for Ni/Si and Hf/Ni/Si structures at a rate of 2°C.

Figure 3-15 shows display temperature of thermocouple as a function of annealing rate. Figure 3-15 was derived from figure 3-12, 3-13 and 3-14.

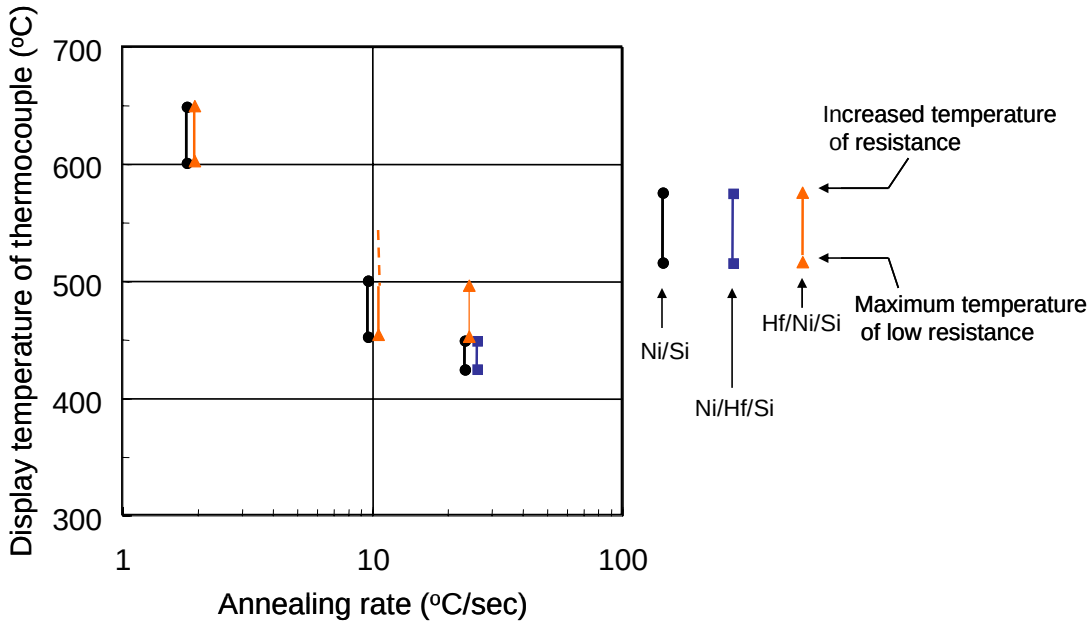

Fig.3-15 Display temperature of thermocouple Sheet resistance vs. annealing rate for Ni/Si, Ni/Hf/Si and Hf/Ni/Si structures.

3.5 Summary of this chapter

In this chapter, we studied metal deposition rate of sputtering system, temperature proofreading of annealing furnace and dependence on annealing rate. It was found that Metal deposition rate depended on DC power, distance from target to sample and deposition time. As a consequence of this, in this study, we determine that DC power supply and distance from target to sample are equal to 150W and 150mm respectively. And film thickness is determined by controlling deposition time. Subsequently, we did temperature proofreading of annealing furnace. We will conform to figure 3-9, when we will conduct RTA. Finally, we investigated dependence on annealing rate. It was found that the critical temperature at which sheet resistance of Ni/Si, Ni/Hf/Si and Hf/Ni/Si structures became higher with decreasing annealing rate.

Chapter 4

Characteristics of Ni silicide by additional Hf layers in long annealing

4.1 Introduction

In this chapter, we investigated characteristics of Hf/Ni/Si, Ni/Hf/Si and Ni/Si structures in long annealing with/without carbon susceptor.

4.2 Fabrication process of Hf/Ni/Si, Ni/Hf/Si and Ni/Si structures

The fabrication processes of Hf/Ni/Si, Ni/Hf/Si and Ni/Si structures are as follows.

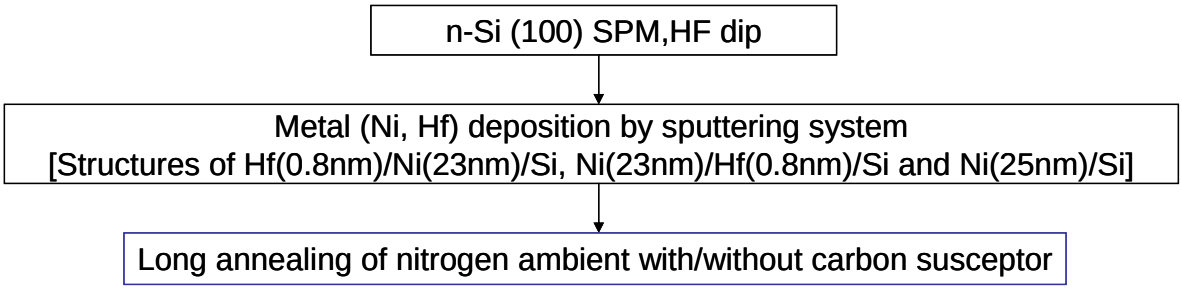

Fig.4-1 Fabrication process of Hf/Ni/Si, Ni/Hf/Si and Ni/Si structures

Figure 4-2 is a view showing a frame format of long annealing conditions.

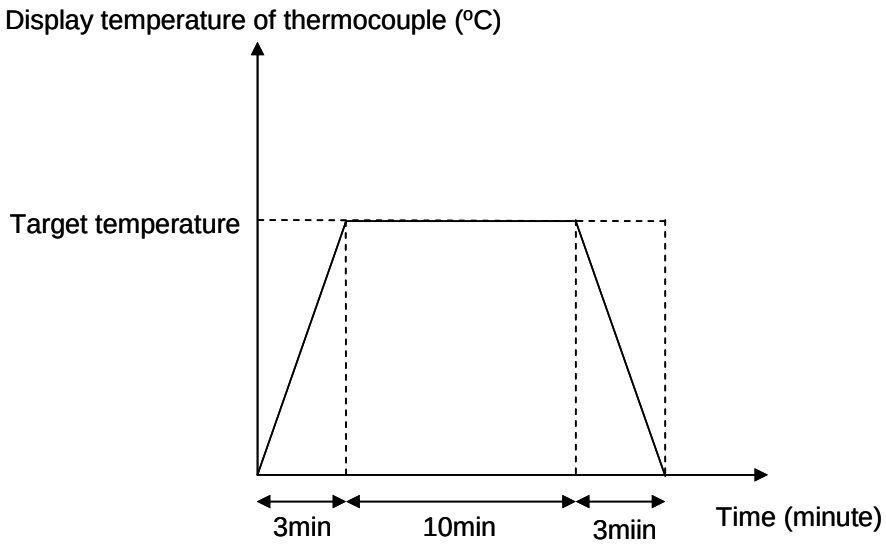

Fig.4-2 Pattern diagrams of long annealing conditions

4.3 Characteristic of Hf/Ni/Si, Ni/Hf/Si and Ni/Si structures with carbon susceptor

Figure 4-3 shows sheet resistance as a function of annealing temperature with carbon susceptor in nitrogen ambient. Hf/Ni/Si and Ni/Hf/Si structures were observed to be low sheet resistance at 500-850^{o}C, while Ni/Si structure was observed as high sheet resistance at 500-850^{o}C in comparison with Hf/Ni/Si and Ni/Hf/Si. Furthermore it was found that Ni/Hf/Si structure was lower than Hf/Ni/Si structure in the case of comparing Ni/Hf/Si and Hf/Ni/Si structures.

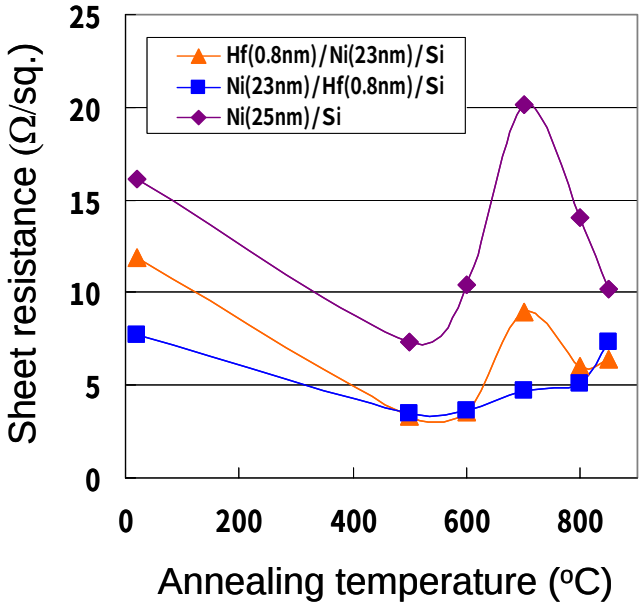

Fig.4-3 Sheet resistance vs. annealing temperature for Hf/Ni/Si, Ni/Hf/Si and Ni/Si structures with carbon susceptor.

Figure 4-4 shows the SEM images for Hf/Ni/Si, Ni/Hf/Si and Ni/Si structures at 500, 700 and 850^{o}C. Hf/Ni/Si and Ni/Hf/Si structures showed smooth surfaces for 500, 700 and 850^{o}C silicidation. On the other hand Ni/Si structure showed rough surface for 500, 700 and 850^{o}C silicidation in comparison with Hf/Ni/Si and Ni/Hf/Si.

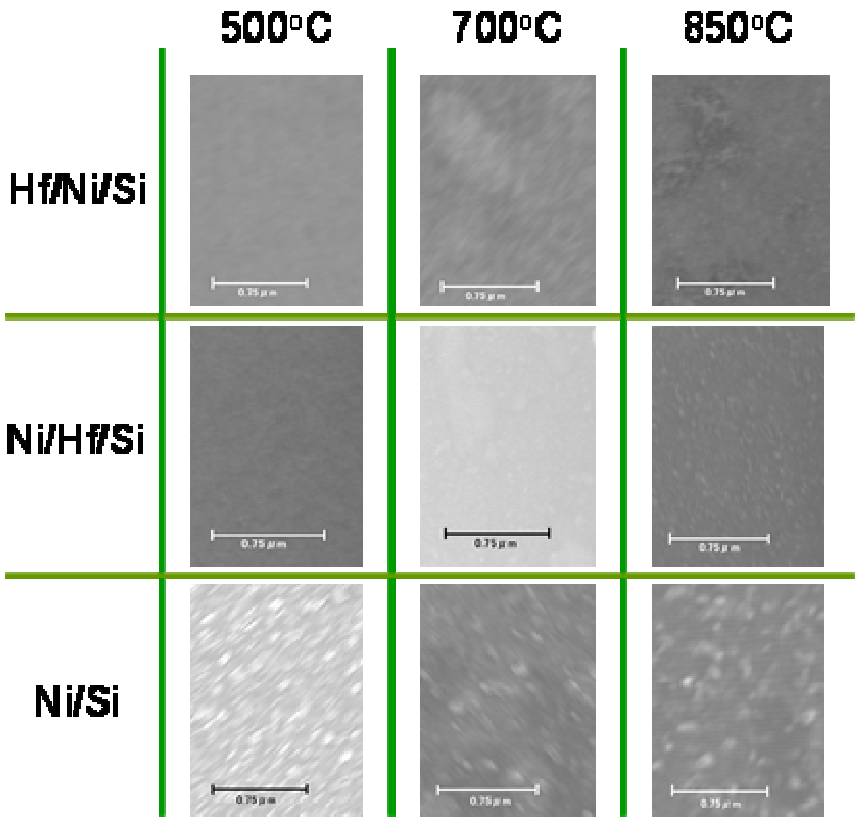

Fig.4-4 SEM images of silicide surfaces for Hf/Ni/Si, Ni/Hf/Si and Ni/Si structures annealed at 500,700 and 850^{o}C.

Figure 4-5 shows the AFM images for Hf/Ni/Si, Ni/Hf/Si and Ni/Si structures at 500, 700 and 850°C. The scan size was 10x10 μm and the z direction was written in figure 4-5. Hf/Ni/Si structure showed smooth surfaces for 500, 700 and 850°C. And Ni/Hf/Si structure showed smooth surfaces for 500 and 700°C. It was found that Hf/Ni/Si structure was smoother than Ni/Hf/Si structure at 850°C. On the other hand Ni/Si structure showed rough surface for 500, 700 and 850°C silicidation in comparison with Hf/Ni/Si and Ni/Hf/Si.

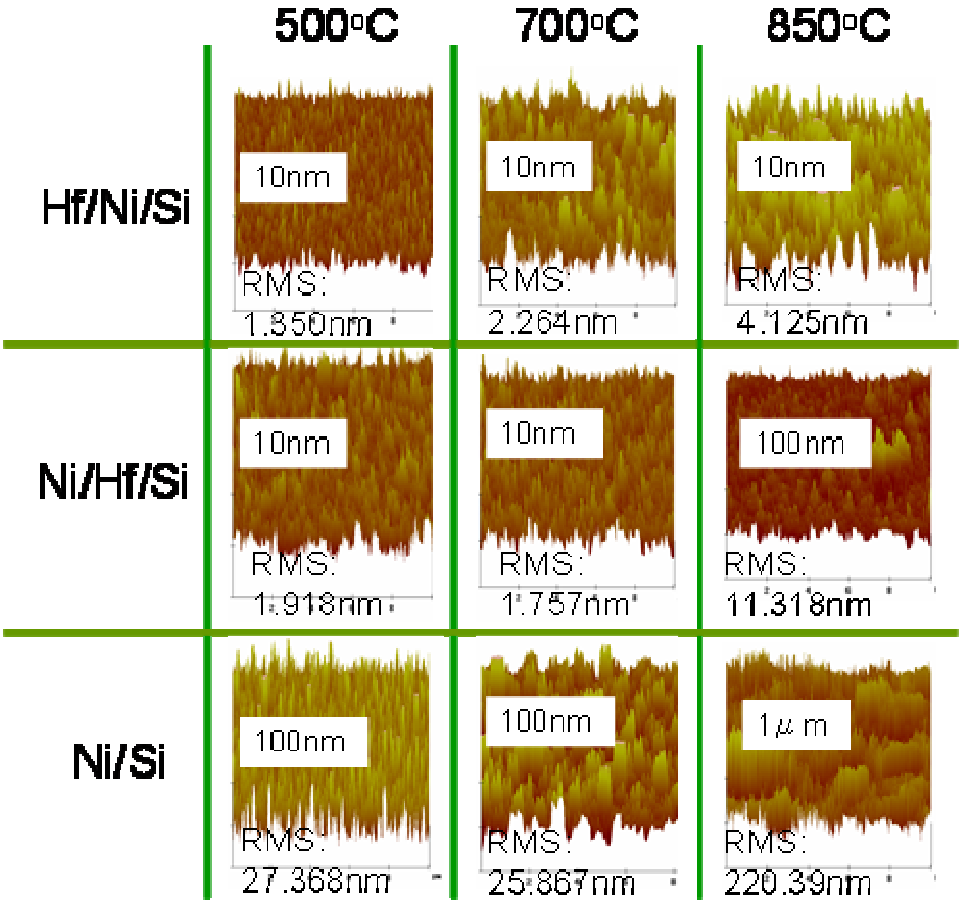

Fig.4-5 AFM images of silicide surfaces for Hf/Ni/Si, Ni/Hf/Si and Ni/Si structures annealed at 500,700 and 850°C.

Figure 4-6 shows RBS spectra of the Hf/Ni/Si, Ni/Hf/Si and Ni/Si structures for as-deposited and after 500-850^{o}C silicidation. It was found that Hf layer moved to surface layer after annealing for Ni/Hf/Si structure. The most of Hf layer were remained without reaction with Ni or Si even after the silicidation annealing. Also uniform NiSi layers were found to be formed for Hf/Ni/Si, Ni/Hf/Si and Ni/Si structures at 500 and 700^{o}C.

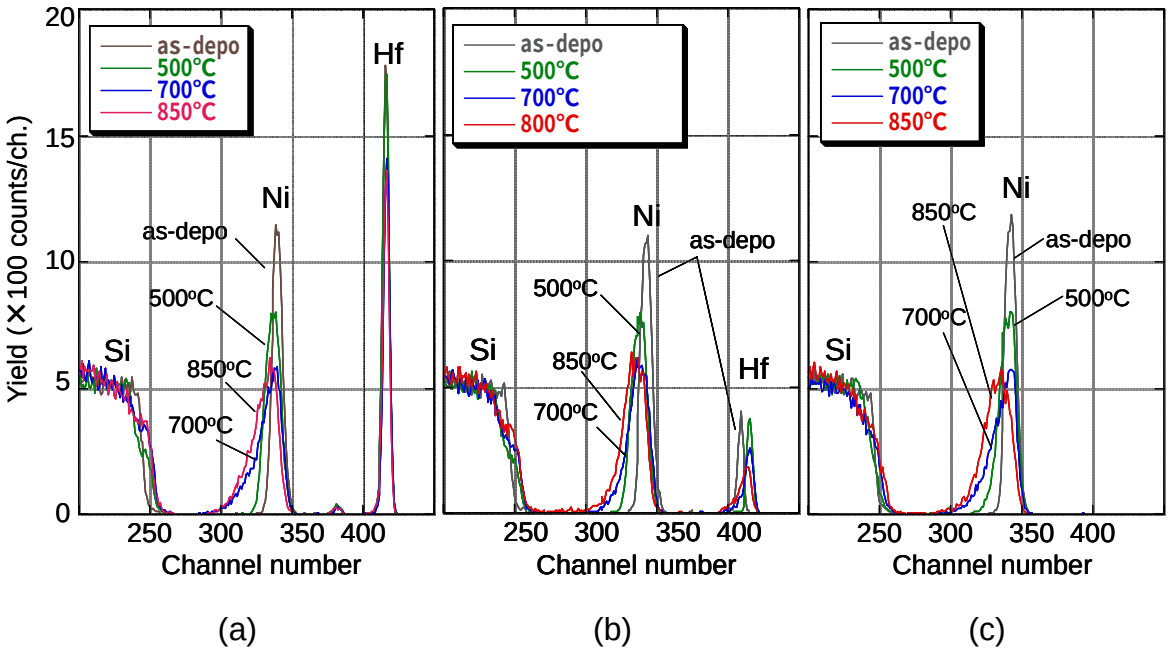

Fig.4-6 RBS spectra of (a) Hf/Ni/Si, (b) Ni/Hf/Si and (c) Ni/Si structures before and after long annealing.

4.4 Characteristic of Hf/Ni/Si, Ni/Hf/Si and Ni/Si structures without carbon susceptor

Figure 4-7 shows sheet resistance as a function of annealing temperature without carbon susceptor in nitrogen ambient. Figure4-7(b) is an expansion of figure 4-7(a). Hf/Ni/Si and Ni/Si structures were observed to be low sheet resistance at 530-670^{o}C, while Ni/Hf/Si structure was observed as high sheet resistance at 670^{o}C. Therefore it was found that thermal stability of Ni/Hf/Si structure was worse than Hf/Ni/Si and Ni/Si structures.

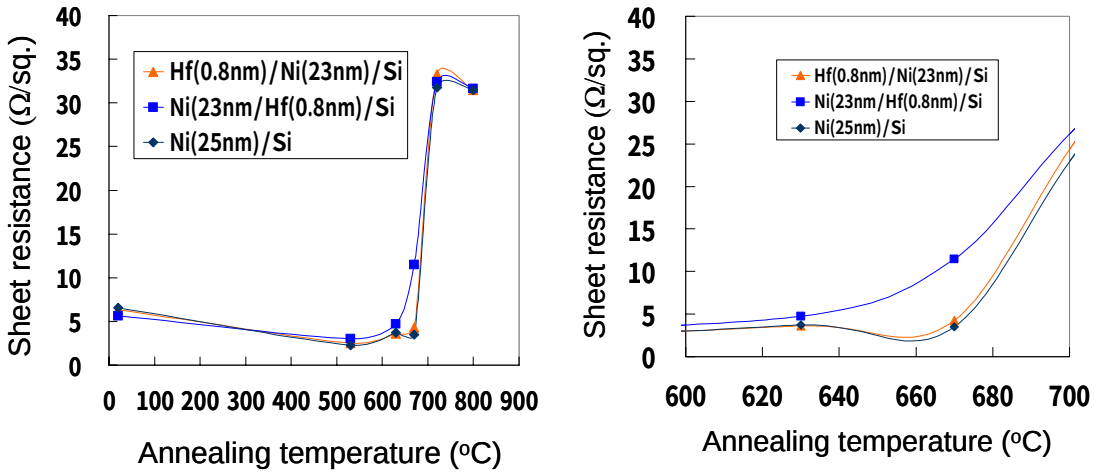

(a) (b)

Fig.4-7 Sheet resistance vs. annealing temperature for Hf/Ni/Si, Ni/Hf/Si and Ni/Si structures without carbon susceptor. Figure4-7(b) is an expansion of figure 4-7(a).

Figure 4-8 shows the SEM images for Hf/Ni/Si, Ni/Hf/Si and Ni/Si structures at 630, 670 and 720^{o}C. Hf/Ni/Si and Ni/Si structures showed smooth surfaces for 630 and 670^{o}C silicidation. However agglomeration was observed for Hf/Ni/Si and Ni/Si structures at 720^{o}C. On the other hand agglomeration was observed for Ni/Hf/Si structure at 670 and 720^{o}C.

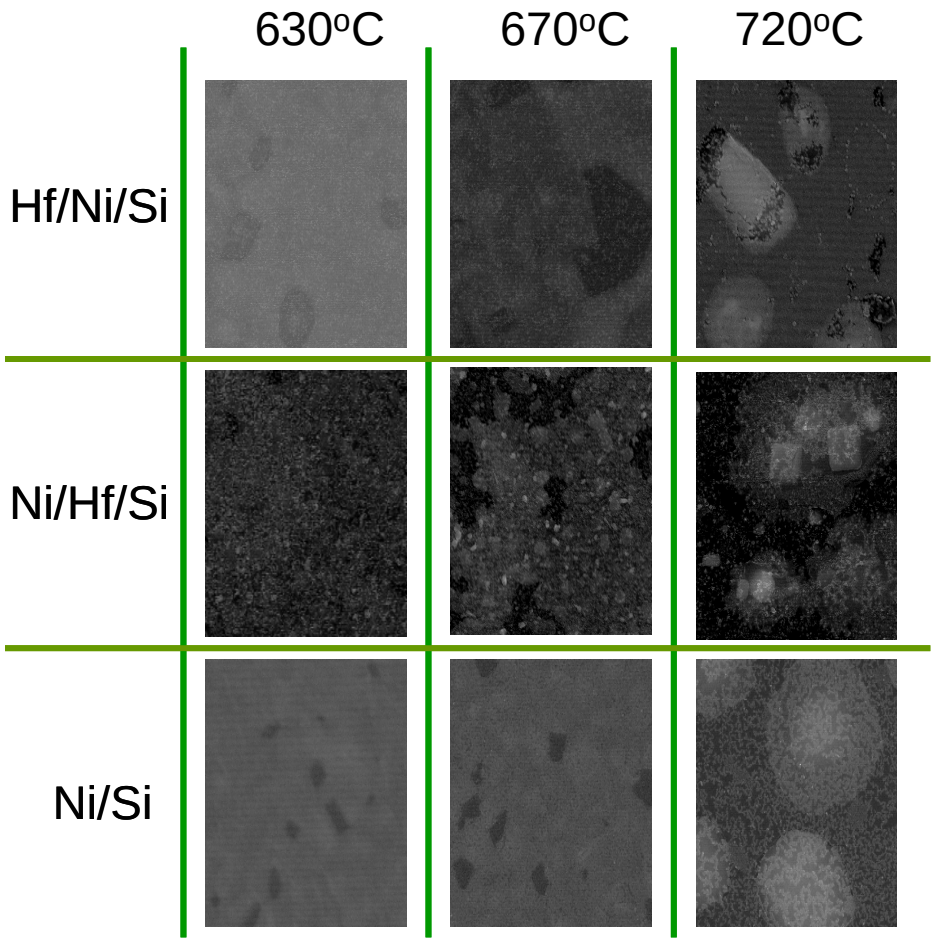

Fig.4-8 SEM images of silicide surfaces for Hf/Ni/Si, Ni/Hf/Si and Ni/Si structures annealed at 630,670 and 720^{o}C.

Figure 4-9 shows the AFM images for Hf/Ni/Si, Ni/Hf/Si and Ni/Si structures at 630, 670 and 720°C. The scan size was 10x10 μm and the z direction was 100nm/div. Hf/Ni/Si structure showed smooth surfaces for 630, 670 and 720°C silicidation in comparison with Ni/Si structures. On the other hand Ni/Hf/Si structure showed rough surfaces for 670 and 720°C silicidation in comparison with Ni/Si structures.

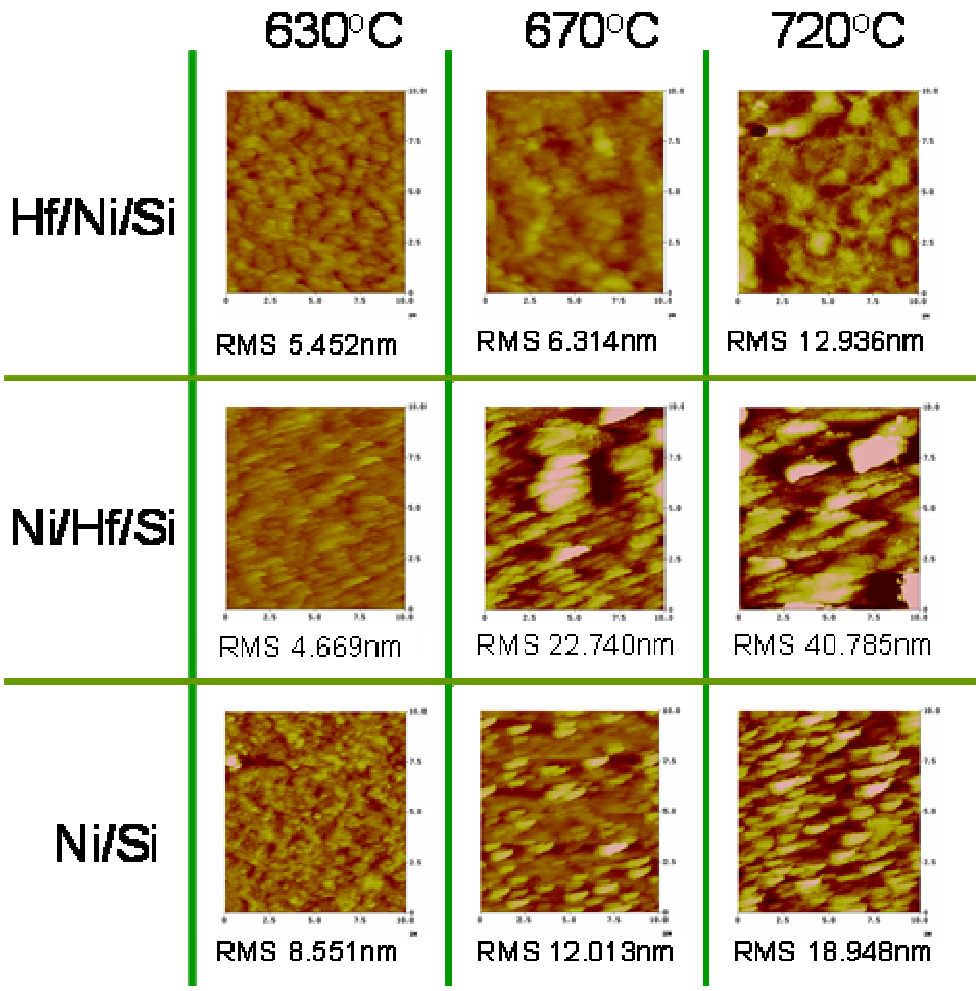

Fig.4-9 AFM images of silicide surfaces for Hf/Ni/Si, Ni/Hf/Si and Ni/Si structures annealed at 630,670 and 720°C.

4.5 Summary of this chapter

In this chapter, we studied long annealing of Hf/Ni/Si, Ni/Hf/Si and Ni/Si structures with/without carbon susceptor.

1) Characteristic of Hf/Ni/Si, Ni/Hf/Si and Ni/Si structures with carbon susceptor

From the viewpoints of sheet resistance, SEM and AFM, It was found that introduction of the Hf thin layer was effective to increase upper limit of silicidation temperature at which low resistive and smooth NiSi layers were obtained, and that Ni/Hf/Si structure has a lower sheet resistance than Hf/Ni/Si structure in the case of comparing Ni/Hf/Si and Hf/Ni/Si structures. And furthermore, from the RBS spectra, in the case of the Hf/Ni/Si structure, shape and position of the peak from Hf was not changed after 500 and 700^{o}C annealing, that is, top Hf layer was remained on the top of NiSi in the form of pure Hf layer. In the case of the Ni/Hf/Si structure, the Hf peak moved from interface position to surface top position and peak shape was the same after the annealing, that is, the initial interface Hf layer was move to surface on the NiSi layer and stayed there in the form of pure Hf layer. It is known that Ni diffuses into Si on the formation of Ni silicides. Thus, it is considered that Ni diffused to Si substrate through the interface Hf layer and NiSi was formed under the Hf layer so as to leave the Hf layer on the top without any reaction involving Hf.

2) Characteristic of Hf/Ni/Si, Ni/Hf/Si and Ni/Si structures without carbon susceptor

From the sheet resistance, it was found that introduction of the Hf thin layer was not effective to increase upper limit of silicidation temperature. Specially the critical temperature of Ni/Hf/Si structure was rather decreased. From the viewpoint of surface morphology, Hf/Ni/Si structure showed smooth surfaces for 630, 670 and 720^{o}C silicidation in comparison with Ni/Si structures. On the other hand Ni/Hf/Si structure showed rough surfaces for 670 and 720^{o}C silicidation in comparison with Ni/Si structures.

Chapter 5

Characteristics of Ni silicide by additional Hf layers in RTA

5.1 Introduction

In this chapter, we investigated characteristics of Hf/Ni/Si, Ni/Hf/Si, Hf/Ni/Hf/Si, Ni/Hf/Ni/Si and Ni/Si structures in RTA. In the cases of Hf/Ni/Si and Ni/Hf/Si structures, we also examined whether Hf layer had dependence of characteristics on the thickness.

5.2 Fabrication process of Hf/Ni/Si, Ni/Hf/Si, Hf/Ni/Hf/Si, Ni/Hf/Ni/Si and Ni/Si structures

The fabrication processes of Hf/Ni/Si, Ni/Hf/Si, Hf/Ni/Hf/Si, Ni/Hf/Ni/Si and Ni/Si structures are as follows.

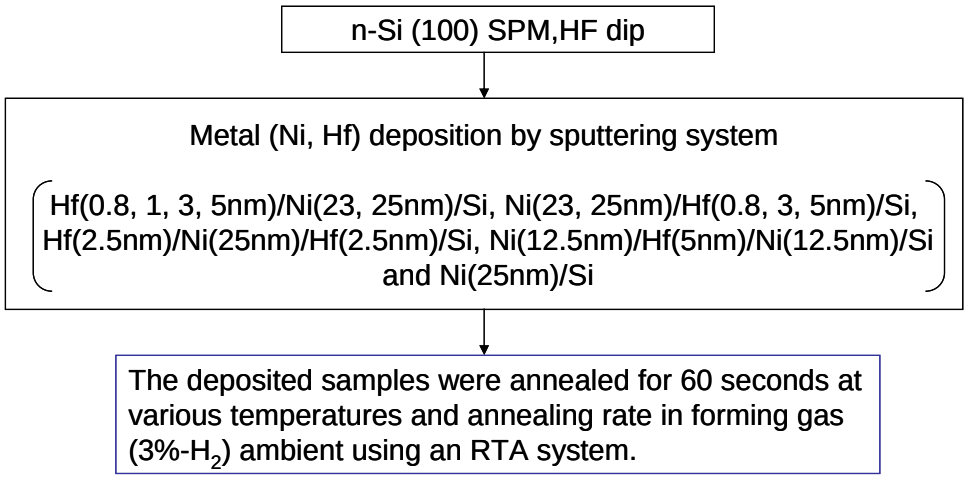

Fig.5-1 Fabrication process of Hf/Ni/Si, Ni/Hf/Si, Hf/Ni/Hf/Si, Ni/Hf/Ni/Si and Ni/Si structures

Figure 5-2 is a view showing a frame format of long annealing conditions.

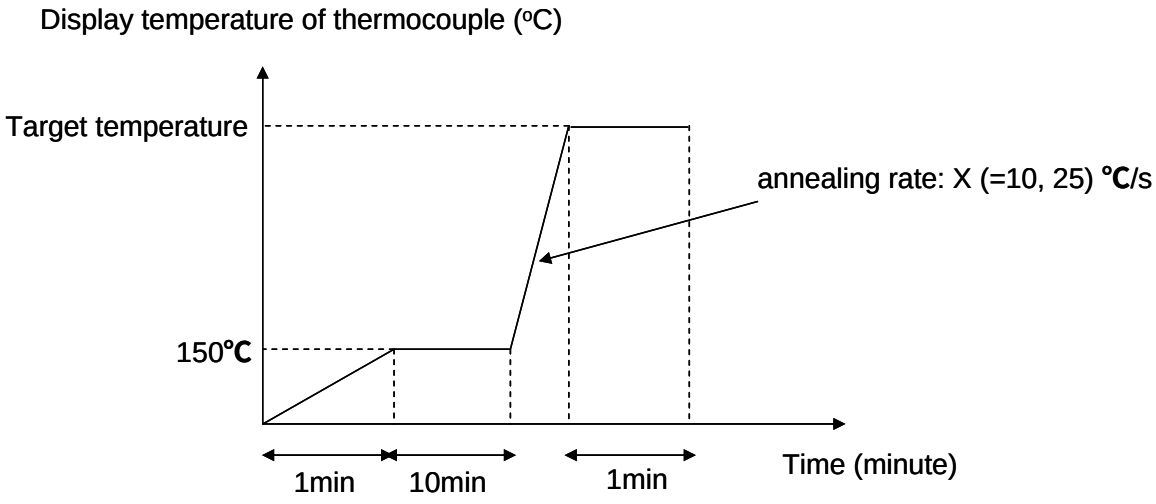

Fig.5-2 Pattern diagrams of RTA conditions

5.3 Characteristic of Hf/Ni/Si, Ni/Hf/Si and Ni/Si structures at a rate of 25°C/s using an RTA system

Figure 5-3 shows sheet resistance as a function of annealing temperature in forming gas (3%-H_2) ambient. Figure5-3(b) is an expansion of figure 5-3(a). Hf/Ni/Si and Ni/Hf/Si structures were observed to be low sheet resistance at 330-500°C, while Ni/Si structure was observed as high sheet resistance at 500°C. And furthermore, it was found that apparent difference of thermal stability between Hf/Ni/Si and Ni/Hf/Si structures was not observed.

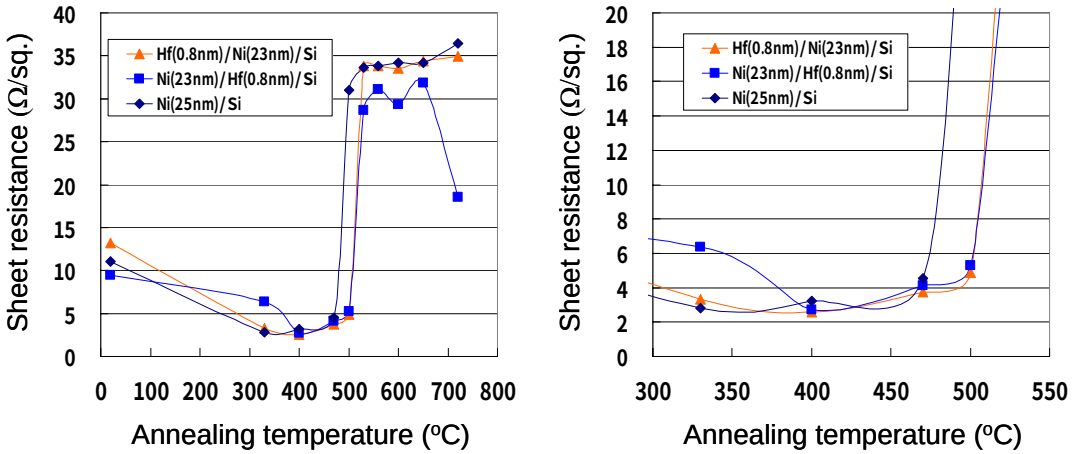

(a) (b)

Fig.5-3 Sheet resistance vs. annealing temperature for Hf/Ni/Si, Ni/Hf/Si and Ni/Si structures at a rate of 25°C using an RTA system. Figure5-3(b) is an expansion of figure 5-3(a).

Figure 5-4 shows the SEM images for Hf/Ni/Si, Ni/Hf/Si and Ni/Si structures at 330, 500 and 600^{o}C. Hf/Ni/Si and Ni/Hf/Si structures showed smooth surfaces for 330 and 500^{o}C silicidation. However agglomeration was observed for Hf/Ni/Si and Ni/Hf/Si structures at 600^{o}C. On the other hand agglomeration was observed for Ni/Hf/Si structure at 500 and 600^{o}C.

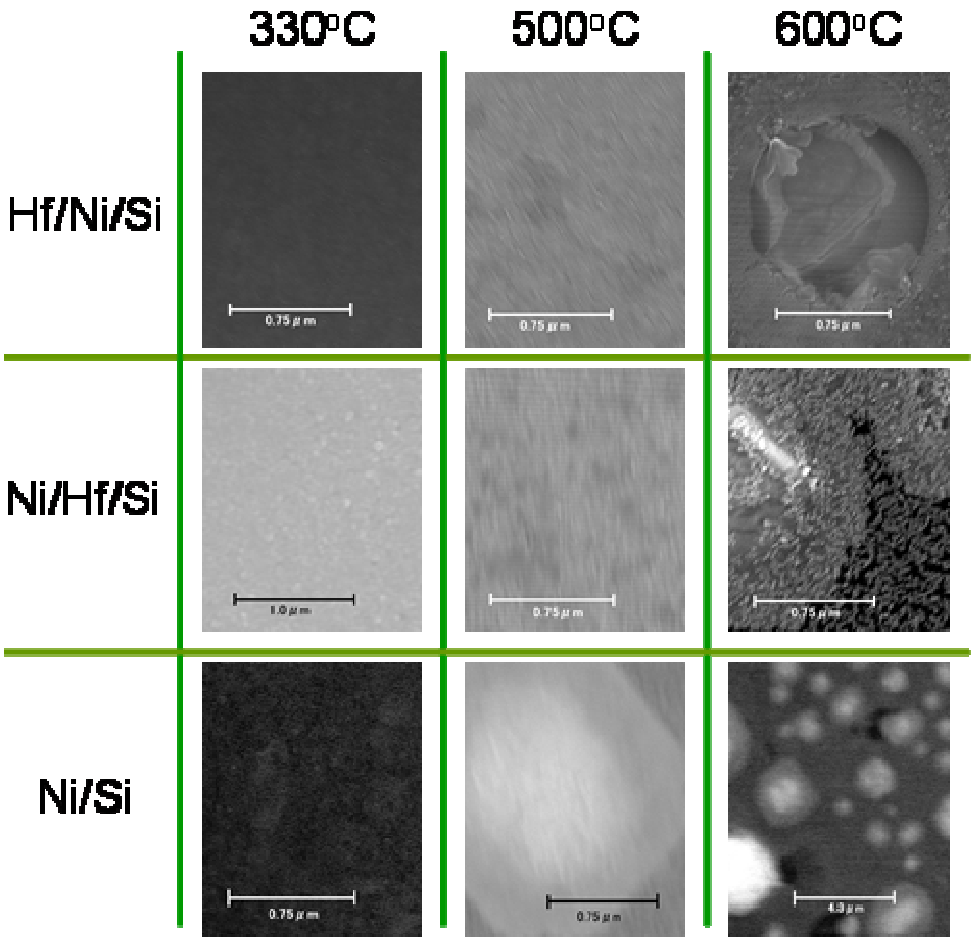

Fig.5-4 SEM images of silicide surfaces for Hf/Ni/Si, Ni/Hf/Si and Ni/Si structures annealed at 330, 500 and 600^{o}C.

Figure 5-5 shows the AFM images for Hf/Ni/Si, Ni/Hf/Si and Ni/Si structures at 330 and 600^{o}C. The scan size was 10x10 μm and the z direction was written in figure 5-5. Hf/Ni/Si, Ni/Hf/Si and Ni/Si structures showed smooth surfaces for 330^{o}C silicidation. Also these structures showed rough surface for 600^{o}C. However it was found that Hf/Ni/Si structure was smooth in comparison with Ni/Hf/Si and Ni/Si structures.

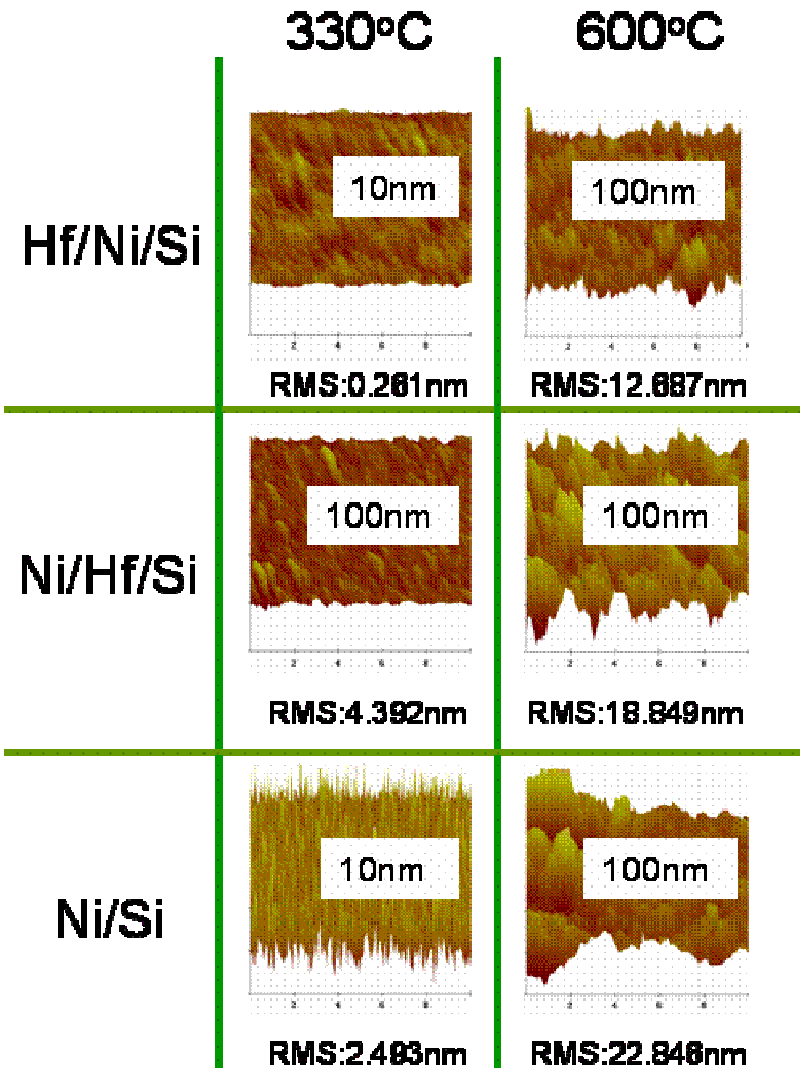

Fig.5-5 AFM images of silicide surfaces for Hf/Ni/Si, Ni/Hf/Si and Ni/Si structures annealed at 330 and 600^{o}C.

Figure 5-6 shows RBS spectra of the Hf/Ni/Si, Ni/Hf/Si and Ni/Si structures for as-deposited and after 400-600^{o}C silicidation. It was found that Hf layer moved to surface layer after annealing for Ni/Hf/Si structure. The most of Hf layer were remained without reaction with Ni or Si even after the silicidation annealing. Also uniform NiSi layers were found to be formed for Hf/Ni/Si, Ni/Hf/Si and Ni/Si structures at 400^{o}C.

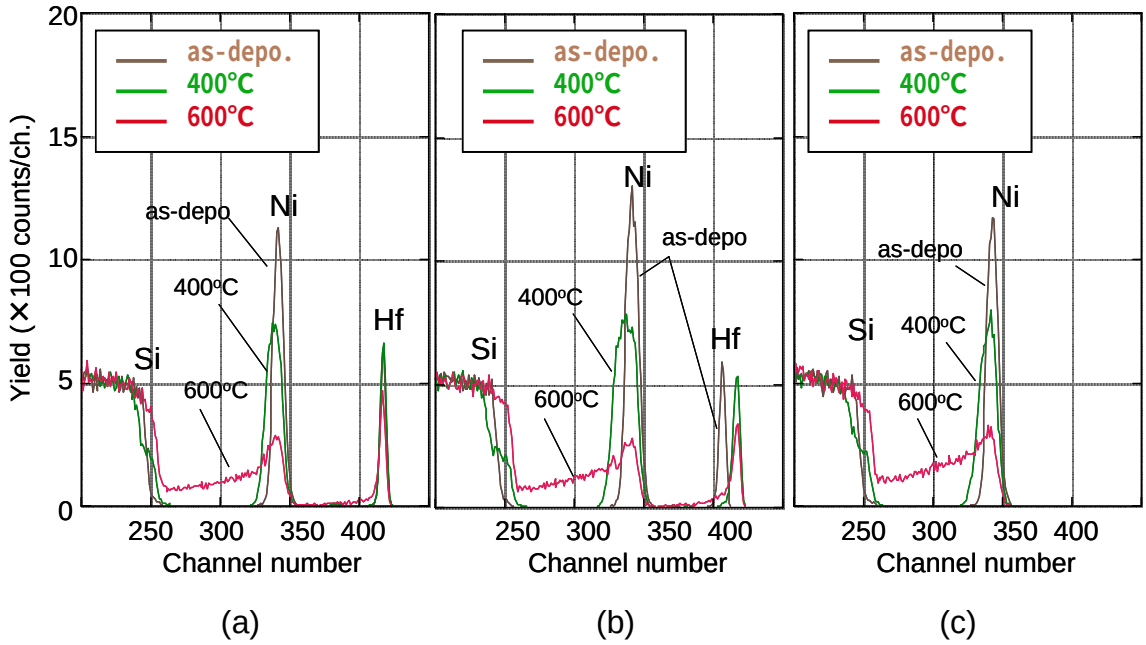

Fig.5-6 RBS spectra of (a) Hf/Ni/Si, (b) Ni/Hf/Si and (c) Ni/Si structures before and after RTA.

5.4 Characteristic of Hf/Ni/Si, Ni/Hf/Si, Hf/Ni/Hf/Si, Ni/Hf/Ni/Si and Ni/Si structures at a rate of 10^{o}C/s using an RTA system

5.4.1 Dependence of characteristics on Hf layer thickness for Hf/Ni/Si, Ni/Hf/Si and Ni/Si structures

Figure 5-7 shows sheet resistance as a function of annealing temperature for Hf/Ni/Si, Ni/Hf/Si and Ni/Si structures, in which thickness of the Hf layer was varied. It was found that critical temperature at which sheet resistance became drastically high for Hf/Ni/Si structures improved about 30^{o}C comparing to Ni/Si reference structure. An advantage of Hf capping layer to thermal stability was observed in this experiment. On the other hand, the critical temperature was rather decreased for Ni/Hf/Si structures. As for the thickness of the Hf layer, apparent dependence on thickness was not observed as far as thickness range examined in this experiment, for both Hf/Ni/Si and Ni/Hf/Si structures.

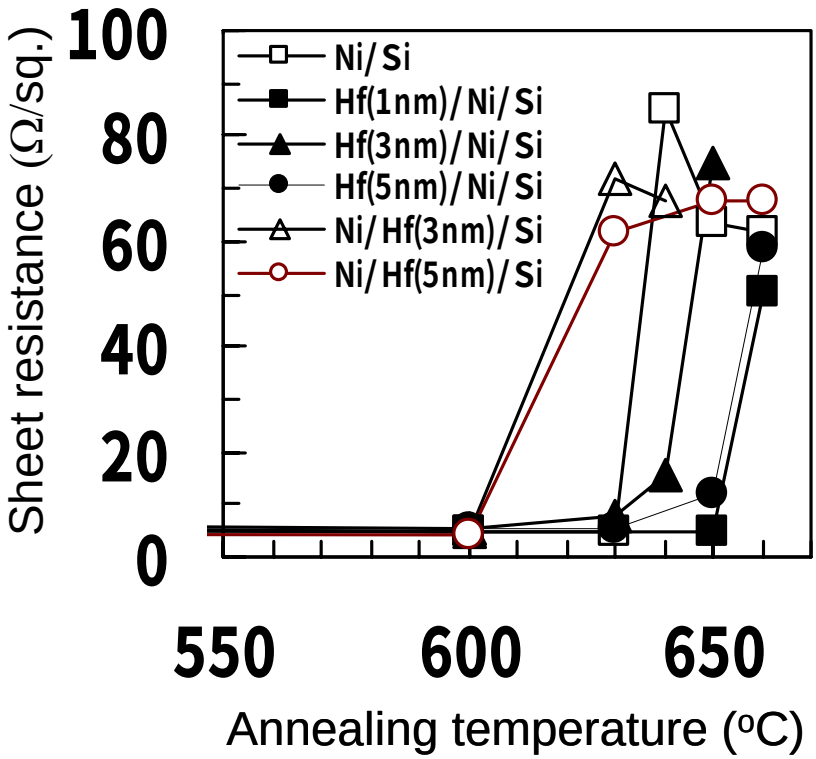

Fig.5-7 Sheet resistance vs. annealing temperature for Hf/Ni/Si, Ni/Hf/Si and Ni/Si structures, in which thickness of the Hf layer was varied.

Figure 5-8 shows the SEM images for Hf/Ni/Si and Ni/Si structures, in which thickness of the Hf layer was varied. Thickness of the Ni layer is 25nm. These samples were annealed at 600-660^{o}C. In Hf(1nm)/Ni/Si structure, smooth surfaces were observed at 600 and 650^{o}C. However agglomeration occurred at 660^{o}C. In Hf(3nm)/Ni/Si structure, smooth surface was observed at 600^{o}C. However, rough surfaces were observed at 630, 640 and 650^{o}C. It was not clear whether agglomeration occurred at 630, 640 and 650^{o}C, as far as we determine it from SEM micrographs. In Hf(5nm)/Ni/Si structure, smooth surface was observed at 600 and 630^{o}C. However, rough surfaces were observed at 650 and 660^{o}C. It was inarticulate whether agglomeration occurred at 650 and 660^{o}C, as

far as we determine it from SEM micrographs. Also we observed Ni/Si structure in order to investigate advantage of the Hf layer. In Ni/Si structure, smooth surfaces were observed at 600 and 630^{o}C. However agglomeration occurred at 660^{o}C. Finally, in Hf (1, 3, 5nm)/Ni/Si and Ni/Si structures, it was found that samples of low resistance region became smooth surface, and that samples of high resistance region became rough surface.

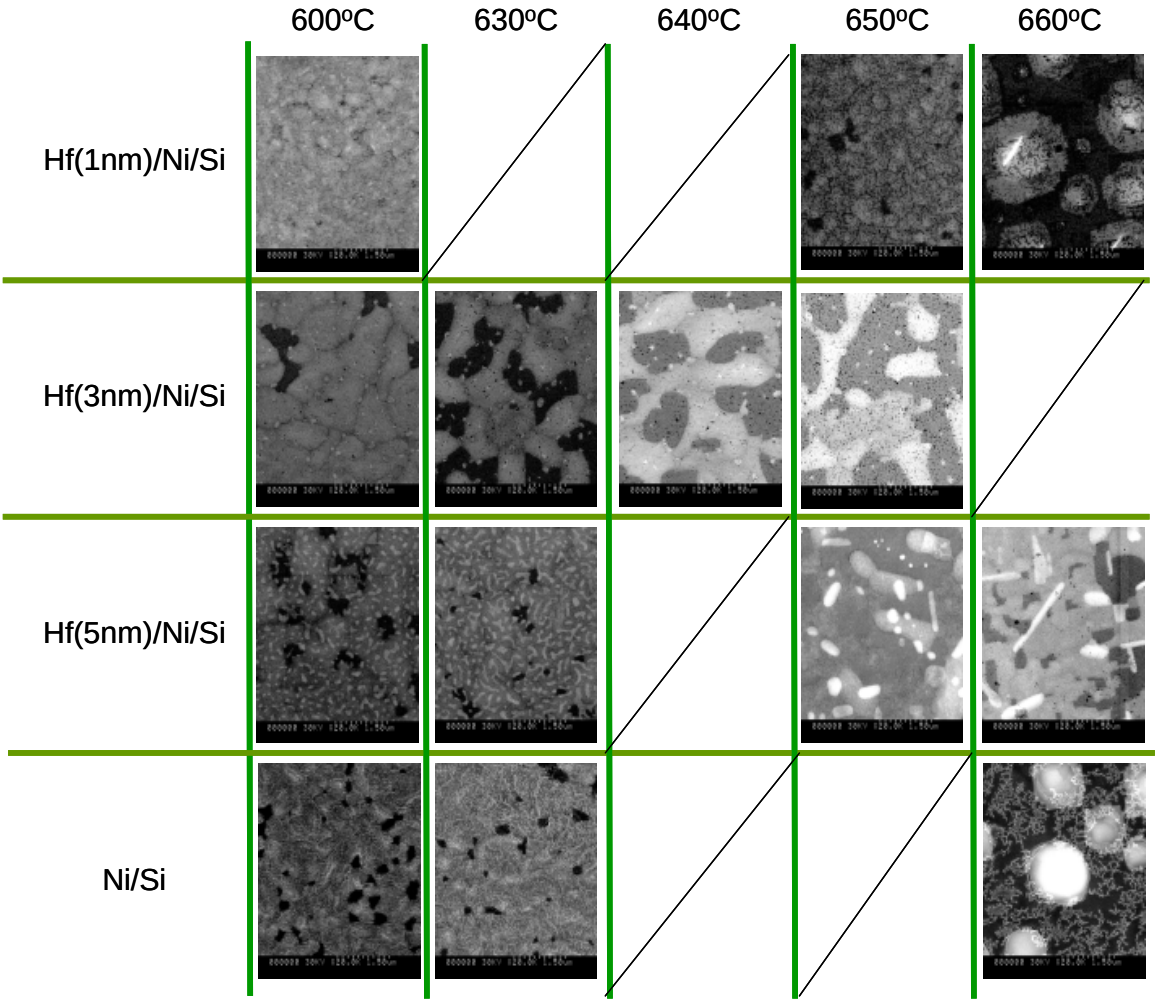

Fig.5-8 SEM images of silicide surfaces for Hf/Ni/Si and Ni/Si structures, in which thickness of the Hf layer was varied. Here, these samples were annealed at 600-660^{o}C.

Figure 5-9 shows the SEM images for Ni/Hf/Si and Ni/Si structures, in which thickness of the Hf layer was varied. Thickness of the Ni layer is 25nm. These samples were annealed at 600-630^{o}C. In Ni/Hf(3nm)/Si structure, smooth surfaces were observed at 600^{o}C. However agglomeration occurred at 630^{o}C. In Ni/Hf(5nm)/Si structure, smooth surface was observed at 600^{o}C. However, rough surfaces were similarly observed at 630^{o}C. Also we used micrographs of Ni/Si structure in common with figure 5-8. Finally, in case of Ni/Hf(3, 5nm)/Si structures, it was found that the temperature of rough surface became rather lower comparing to the Ni/Si reference structure.

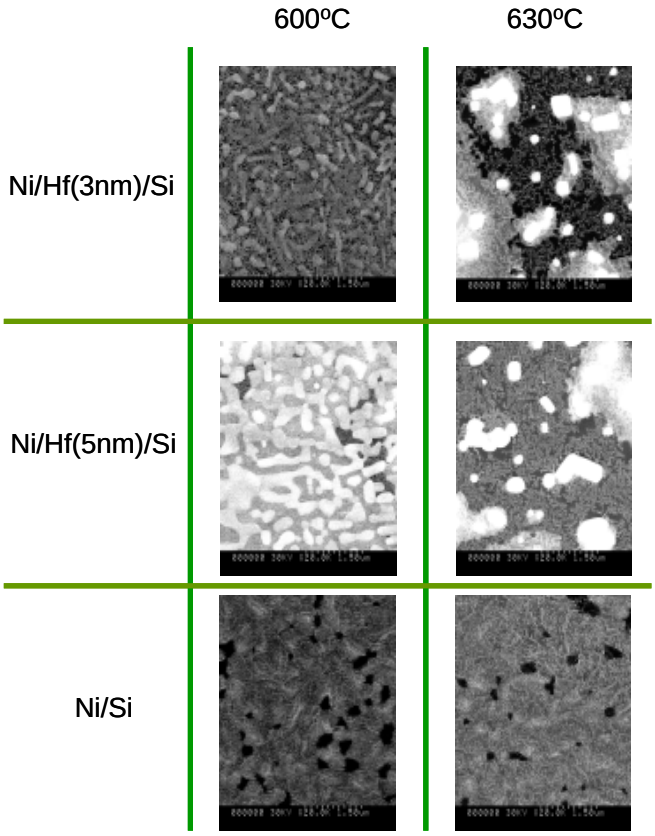

Fig.5-9 SEM images of silicide surfaces for Ni/Hf/Si and Ni/Si structures, in which thickness of the Hf layer was varied. Here, these samples were annealed at 600-630^{o}C.

5.4.2 Characteristic of Hf/Ni/Hf/Si and Ni/Hf/Ni/Si structures

Figure 5-12 shows sheet resistance as a function of annealing temperature for Hf/Ni/Hf/Si, Ni/Hf/Ni/Si and Ni/Si structures. Figure5-12(b) is an expansion of figure 5-12(a).It was found that critical temperature at which sheet resistance became drastically high for Hf/Ni/Hf/Si structure improved about 50^{o}C comparing to Ni/Si reference structure. An advantage of Hf/Ni/Hf/Si structure to thermal stability was observed in this experiment. On the other hand, the critical temperature was hardly changed for Ni/Hf/Ni/Si structures comparing to Ni/Si reference structure. However, Ni/Hf/Ni/Si structure was lower than Ni/Si structure at 650 and 660^{o}C in the case of comparing Ni/Hf/Ni/Si and Ni/Si structures.

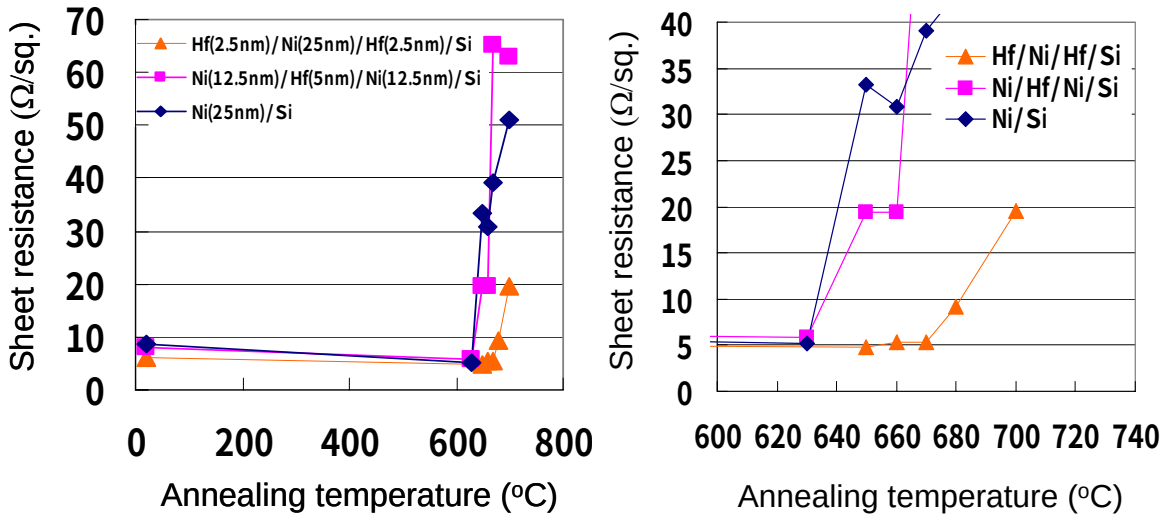

Fig.5-12 Sheet resistance vs. annealing temperature for Hf/Ni/Hf/Si, Ni/Hf/Ni/Si and Ni/Si structures at a rate of 10^{o}C using an RTA system. Figure5-12(b) is an expansion of figure 5-12(a).

Figure 5-13 shows the SEM images for Hf(2.5nm)/Ni(25nm)/Hf(2.5nm)/Si, Ni(12.5nm)/Hf(5nm)/Ni(12.5nm)/Si and Ni(25nm)/Si structures. These samples were annealed at 600-700^{o}C. In Hf/Ni/Hf/Si structure, smooth surfaces were observed at 650 and 680^{o}C. However, rough surfaces were observed at 700^{o}C. It was not clear whether agglomeration occurred at 700^{o}C, as far as we determine it from SEM micrographs. In Ni/Hf/Ni/Si structure, smooth surface was observed at 630^{o}C. However, agglomeration occurred at 650 and 700^{o}C. Also we used micrographs of Ni/Si structure in common with figure 5-8. Finally, it was found that Hf/Ni/Hf/Si structure kept smooth surface until high temperature region in comparison with Ni/Si structure.

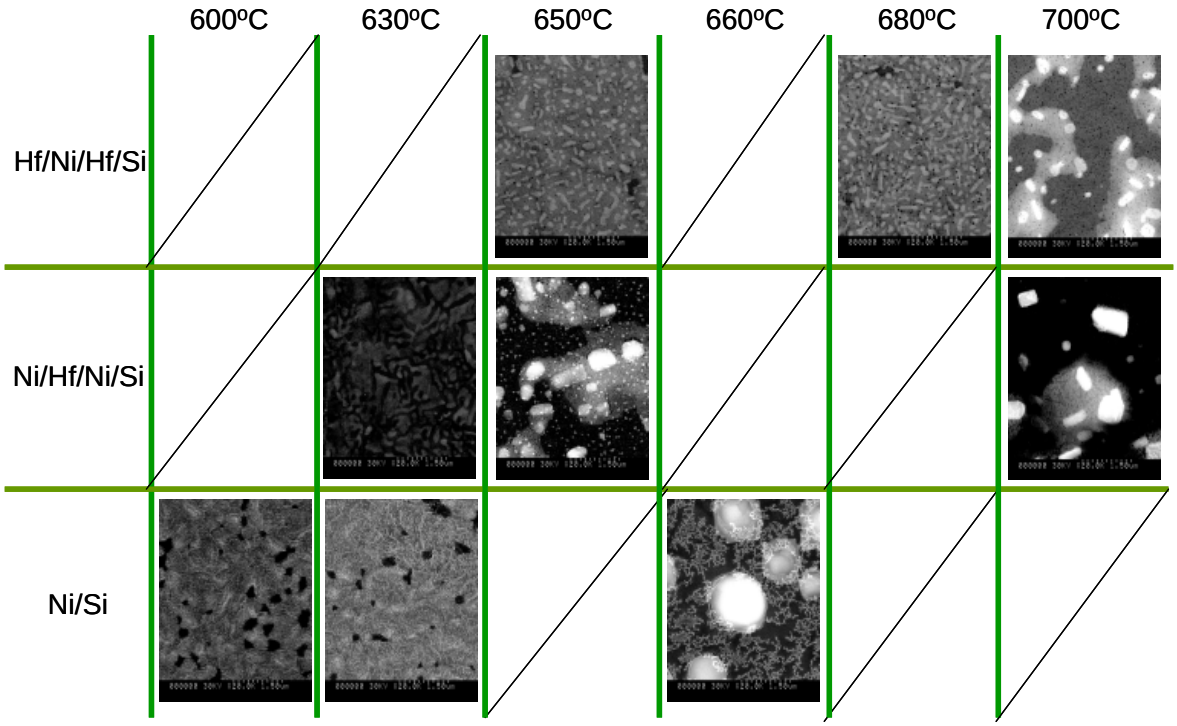

Fig.5-13 SEM images of silicide surfaces for Hf(2.5nm)/Ni(25nm)/Hf(2.5nm)/Si, Ni(12.5nm)/Hf(5nm)/Ni(12.5nm)/Si and Ni(25nm)/Si structures. Here, these samples were annealed at 600-700^{o}C.

5.5 Summary of this chapter

In this chapter, we investigated characteristics of Hf/Ni/Si, Ni/Hf/Si, Hf/Ni/Hf/Si, Ni/Hf/Ni/Si and Ni/Si structures in RTA. In the cases of Hf/Ni/Si and Ni/Hf/Si structures, we also examined whether Hf layer had dependence of characteristics on the thickness.

1) Characteristic of Hf/Ni/Si, Ni/Hf/Si and Ni/Si structures at a rate of 25^{o}C/s using an RTA system

From the viewpoints of sheet resistance, SEM and AFM, It was found that introduction of the Hf thin layer was effective to increase upper limit of silicidation temperature at which low resistive and smooth NiSi layers were obtained. Furthermore, from the RBS spectra, in the case of the Hf/Ni/Si structure, shape and position of the peak from Hf was not changed after 400 and 600^{o}C annealing, that is, top Hf layer was remained on the top of NiSi in the form of pure Hf layer. In the case of the Ni/Hf/Si structure, the Hf peak moved from interface position to surface top position and peak shape was the same after the annealing, that is, the initial interface Hf layer was move to surface on the NiSi layer and stayed there in the form of pure Hf layer. It is considered that Ni diffused to Si substrate through the interface Hf layer and NiSi was formed under the Hf layer so as to leave the Hf layer on the top without any reaction involving Hf in common with chapter 4.

2) Characteristic of Hf/Ni/Si, Ni/Hf/Si, Hf/Ni/Hf/Si, Ni/Hf/Ni/Si and Ni/Si structures at a rate of 10^{o}C using an RTA system

It was found that critical temperature at which sheet resistance became drastically high for Hf/Ni/Si structures improved about 30^{o}C comparing to Ni/Si reference structure. In Hf(1nm)/Ni/Si structure, smooth surfaces were observed until 650^{o}C. On the other hand, the critical temperature was rather decreased for Ni/Hf/Si structures comparing to the Ni/Si reference structure. In case of Ni/Hf(3, 5nm)/Si structures, it was found that the temperature of rough surface became rather lower comparing to the Ni/Si reference structure. Finally, as for the thickness of the Hf layer, apparent dependence on thickness was not observed as far as thickness range examined in this experiment for both Hf/Ni/Si and Ni/Hf/Si structures. In Hf/Ni/Hf/Si structure, it was found that critical temperature at which sheet resistance became drastically high improved about 50^{o}C comparing to the Ni/Si structure, and that Hf/Ni/Hf/Si structure kept smooth surface until 680^{o}C. Lastly, it was found that Ni/Hf/Ni/Si structure was not effective to increase upper limit of silicidation temperature.

Chapter 6

Conclusion

In this chapter, we will conclude of this study and describe the future issue.

6.1 Result of this work

In this study, we aim to improve thermal stability of NiSi layer by additional Hf layers.

The conclusions of this study are as follows:

The first, we investigated characteristics of Hf/Ni/Si, Ni/Hf/Si and Ni/Si structures in long annealing with/without carbon susceptor. From characteristic of Hf/Ni/Si, Ni/Hf/Si and Ni/Si structures with carbon susceptor, it was found that introduction of the Hf thin layer was effective to increase upper limit of silicidation temperature at which low resistive and smooth NiSi layers were obtained, and that Ni/Hf/Si structure has a lower sheet resistance than Hf/Ni/Si structure in the case of comparing Ni/Hf/Si and Hf/Ni/Si structures. And furthermore, from the RBS spectra, in the case of the Hf/Ni/Si structure, shape and position of the peak from Hf was not changed after annealing, that is, top Hf layer was remained on the top of NiSi in the form of pure Hf layer. In the case of the Ni/Hf/Si structure, the Hf peak moved from interface position to surface top position and peak shape was the same after the annealing, that is, the initial interface Hf layer was move to surface on the NiSi layer and stayed there in the form of pure Hf layer. It is known that Ni diffuses into Si on the formation of Ni silicides. Thus, it is considered that Ni diffused to Si substrate through the interface Hf layer and NiSi was formed under the Hf layer so as to leave the Hf layer on the top without any reaction involving Hf.

The second, we investigated characteristic of Hf/Ni/Si, Ni/Hf/Si and Ni/Si structures without carbon susceptor. From the sheet resistance, it was found that introduction of the Hf thin layer was not effective to increase upper limit of silicidation temperature. Specially the critical temperature of Ni/Hf/Si structure was rather decreased.

The third, we investigated characteristic of Hf/Ni/Si, Ni/Hf/Si and Ni/Si structures at a rate of 25^{o}C/s using an RTA system. From the viewpoints of sheet

resistance, SEM and AFM, It was found that introduction of the Hf thin layer was effective to increase upper limit of silicidation temperature at which low resistive

and smooth NiSi layers were obtained.

The fourth, we investigated characteristic of Hf/Ni/Si, Ni/Hf/Si, Hf/Ni/Hf/Si, Ni/Hf/Ni/Si and Ni/Si structures at a rate of 10^{o}C using an RTA system. It was found that critical temperature at which sheet resistance became drastically high for Hf/Ni/Si structures improved about 30^{o}C comparing to Ni/Si reference structure. On the other hand, the critical temperature was rather decreased for Ni/Hf/Si structures comparing to the Ni/Si reference structure. And as for the thickness of the Hf layer, apparent dependence on thickness was not observed as far as thickness range examined in this experiment for both Hf/Ni/Si and Ni/Hf/Si structures. In Hf/Ni/Hf/Si structure, it was found that critical temperature at which sheet resistance became drastically high improved about 50^{o}C comparing to the Ni/Si structure, and that Ni/Hf/Ni/Si structure was not effective to increase upper limit of silicidation temperature.

6.2 Future issues

From the RBS spectra, in the case of the Ni/Hf/Si structure, it is considered that Ni diffused to Si substrate through the interface Hf layer and NiSi was formed under the Hf layer so as to leave the Hf layer on the top without any reaction involving Hf. We felt this to be cause, which had weak reactivity of Hf and Si. If we used metal, which had strong reactivity with Si, Ni did not diffuse to Si substrate through the interface this metal layer. As a result, it is considered that thermal stability of NiSi is better than result of this study.

Acknowledgements

The author would like to give the greatest thanks to Professor Hiroshi Iwai got his thorough instruction.

The author would like to thank Associate Professor Kazuo Tsutsui for his extensive advice, valuable discussions and continuous supports.

The author would like to thank Associate Professor Shun-ichiro Ohmi for his extensive advice, valuable discussions and continuous supports.

The author would like to thank Associate Professor Hiroshi Ishiwara for his extensive advice, valuable discussions and continuous supports.

The author would like to thank Dr. Koji Aizawa very much who supported his researches.

The author would like to thank Associate Professor Tetsuji Yano very much who supported his researches.

The author would like to thank Mr. Dai. Shouji very much who supported his researches.

The author would be much grateful to all members of Professor Ishiwara, Tokumitu, Tsutsui, Sakai and Ohmi Laboratory, for their providing with the use of their equipments and taking care of them.

The author would like to thank research colleagues of Professor Iwai's Laboratory, Mr. J. Tonotani, Mr. K. Ohshima, Mr. Y. Kim, Mr. Jin Aun NG, Mr. A. Kuriyama, Mr. Y. Sasaki, Mr. Molina Reyes Joel, Mr. K Sasaki, Mr. Hendriansyah Sauddin, T. Satou, Mr. K. Miyauchi, Mr. Yoshida, Mr. K Takagi, I. Aiba, Mr. K. Nakagawa, Mr. A. Fukuyama, Mr. Y. Kuroki, Mr. S. Yoshizaki, Mr. XIANG Ruifei, Mr. Kim TaeWan and Mr. K. Nagahiro for the kind friendship and active

discussions.

The author would like to express science gratitude to laboratory secretaries, Ms. Y. Hashizume, Ms. A. Matsumoto, Ms. N. Hayashi and Ms. N. Iizukaka.

This study was partially supported by ULSI Process Technology Development Center, Semiconductor Company, Matsushita Electric. The author would like to thank Mr. Y. Okuno, M. Matsumoto and Mr. M. Kubota for useful discussions and advice for this study.

This study was partially supported by Grant-in-Aid for Science Research Priority Areas (A): Highly Fictionalized Global Interface Integration.

Finally, the author would like to thank his parents and brother for their warm supported and encouragement.

Youichi Kobayashi,
Yokohama,
March 2005.

Reference

[1] International Technology Roadmap for Semiconductors: 2003 (International SEMATECH, 2003).

[2] K. Macx, Mater. Sci. Eng., R., R11, 53 (1993).

[3] R. Beyers and R. Sinclair, J.Appl. Phys., 57, 5240 (1985).

[4] Z. Ma and L.H. Allen, Phys. Rev. B. 49, 13501 (1994).

[5] E.G.Colgan, J.P. Gambino, and Q. Z. Hong, Mater. Sci. Eng., R., 16, (1996).

[6] F. Deng, R. A. Johnson, P. M. Asbeck and S. S. Lau, J. Appl. Phys., 81, 8047 (1997)

[7] J. B. Lasky, J. S. Nakos, O. J. Cain and P. J. Geiss, IEEE Trans, Electron Devices. ED-38, 262 (1991)

[8] E. G. Colgan, Thin Solid Films, 279, 194 (1996).

[9] P. S. Lee, K.L. Pey, D. Mangelinck, J. Ding, D. Z. Chi and L. Chan, IEEE Electron Device Lett., 22, 568 (2001).

[10] D.X. Xu, S. R. Das, C. J. Peters and L.E.Erickson, Thin Solid Films, 326, 143 (1998).

[11] J. F. Liu, H. B. Chen, J. Y. Feng and J. Zhu, Appl. Phys. Lett., 77, 2177 (2000).

[12] J. F. Liu, J. Y. Feng and J. Zhu, Appl. Phys. Lett., 80, 270 (2002).

[13] L. W. Cheng, S. L. Cheng, L. J. Chen, H. C. Chien, H. L. Lee and F. M. Pan, J. Vac. Sci. Technol. A, 18, 1176 (2000).

[14] D. Mangelinck, J. Y. Dai, J. S. Pan and S. K. Lahiri, Appl. Phys. Lett., 75, 1736 (1999).

[15] R. N. Wang, J. Y. Feng and Y.Huang, Appl. Surf. Sci., 207, 139 (2003).

[16] P. Gergaud, O. Thomas and B. Chenevier, J. Appl. Phys., 94, 1584 (2003).

[17] P. Gergaud, M. Megdiche, O. Thomas and B. Chenevier, Appl. Phys. Lett., 83, 1334 (2003).

[18] C. J. Tsai, P. L. Chung and K. H. Yu, Thin Solid Films, 365, 72 (2000).

[19] J. S. Maa, Y. Ono, D. J. Tweet, F. Zhang and S. T. Hsu, J. Vac. Sci. Technol. A, 19, 1595 (2001).

[20] Tsung Lin Lee, Jam Wem Lee, Mei Chi Lee, Tan Fu Lei and Chung Len Lee, Electrochemical and Solid-State Letters, 6(5), G66 (2003).